

pubs.acs.org/crystal Article

Efficient Polymorph Screening through Crystallization from Bulk and Confined Melts

Published as part of a Crystal Growth and Design virtual special issue Celebrating John N. Sherwood, Pioneer in Organic and Molecular Crystals

Noalle Fellah, Lamia Tahsin, Carolyn Jin Zhang, Bart Kahr, Michael D. Ward, and Alexander G. Shtukenberg*



Cite This: https://doi.org/10.1021/acs.cgd.2c01065

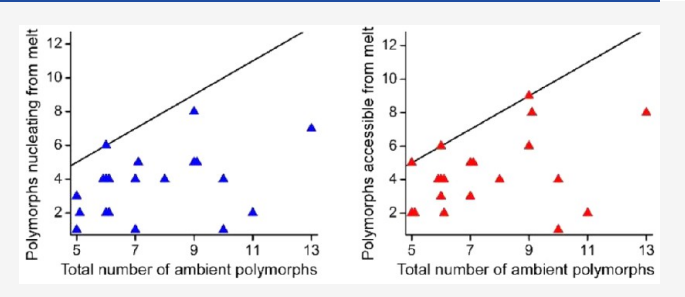


ACCESS |

III Metrics & More

Article Recommendations

ABSTRACT: Crystallization from the melt can allow the achievement of high driving force for crystallization accompanied by relatively slow growth, nucleation, and transformation rates, features that favor its use as an efficient polymorph screening method. Surprisingly, even though melt crystallization has a long history, it has been employed less often in the search for new polymorphs than solution crystallization. Applications of melt crystallization to 21 highly polymorphic, well-characterized compounds with at least five ambient polymorphs revealed that melt crystallization afforded more than half of the known



polymorphs and in many cases revealed new polymorphs not detected by other screening methods. A statistical analysis revealed that polymorphs grown from the melt have a greater propensity for high Z' values, which are not easily accessible by other crystallization protocols and are often not detectable by crystal structure prediction methods. Melt crystallization within nanopores (8–100 nm) performed for 19 of the 21 compounds mostly resulted in polymorphs that dominated crystallization from the bulk melt at similar temperatures. The total number of polymorphs observed in nanopores was less than that observed during crystallization from the bulk melt, however, and melt crystallization under confinement revealed new polymorphs not detected by other crystallization methods.

■ INTRODUCTION

Polymorphism, the ability of a compound to crystallize in two or more crystal structures, is a common feature of molecular crystals. Polymorphs can spontaneously transform into one another (excluding the thermodynamically preferred form). Due to the behavior and distinct properties of polymorphs, several key technologies, including pharmaceuticals, organic semiconductors,² and energetic materials³ can benefit from the discovery and study of all possible polymorphs. The search for new polymorphs (a.k.a. screening) typically involves a variety of methods, including sublimation, growth from solution (solvent evaporation, temperature lowering, mixing with antisolvents, slurrying), solid-state crystallization (exposure to solvent vapors, grinding, and heating/cooling cycles), crystallization directly from the melt, crystallization in the presence of additives, crystallization on tailored substrates, and crystallization under nanoconfinement. 4-6 Regulation of temperature and pressure expands the toolkit for each of these methods as well.

Currently, crystallization from the melt plays a relatively minor role in polymorph screening workflows in industry,⁷

which is puzzling given the long history of melt crystallization of materials, including molecular crystals. ^{8–12} In recent years, a shift has occurred toward the recognition of melt crystallization as an important method for studying molecular crystals and their polymorphism. Crystallization at the microgram scale performed from melt microdroplets has emerged as a tool for cultivating single crystals for structure solution. ¹³ Recently, our laboratory has demonstrated the value of melt crystallization through the discovery of new polymorphs of common well-characterized materials such as paracetamol, ¹⁴ testosterone propionate, ¹⁵ resorcinol, ¹⁶ aspirin, ¹⁷ coumarin, ¹⁸ DDT, ¹⁹ benzamide, ²⁰ isoniazid, ²¹ and imidacloprid, ²² among others. Nonetheless, many questions remain: (i) What percentage of all observed polymorphs are accessible through melt

Received: September 21, 2022 Revised: November 7, 2022



Scheme 1. Molecular Structure of Studied Compounds

crystallization? (ii) How many polymorphs achieved by melt crystallization are truly inaccessible by others methods? (iii) Which polymorphs are more likely to be found by melt crystallization? (iv) What material properties favor polymorph discovery through melt crystallization screening?

Crystallization performed under confinement in nanopores with diameters ranging from 3 to 200 nm has been demonstrated to be a powerful, albeit not routinely used, method for studying polymorphism, ^{23–25} often producing new polymorphs^{22,26} and altering polymorph stability rankings. ^{20,21,27,28} This prompts new questions, including the following: (i) Are polymorph outcomes different for crystallization of a bulk melt compared with the corresponding melts in nanopores? (ii) How often does crystallization under confinement produce new polymorphs? (iii) How stable—thermodynamically and kinetically—are particular polymorphs under confinement, and what are the stability limits that permit detection of metastable forms?

Herein, we describe efforts which address these questions by comparing the phase behavior of 21 highly polymorphic materials (≥5 reported ambient polymorphs) grown from their respective bulk melts and melts confined within nanopores. The materials were either chosen from the literature ^{12,29,30} or are representative examples from our laboratory ^{14,18,22,31} (Scheme 1). This is only a subset of compounds with five or more ambient polymorphs, and other examples are summarized in Table 1. The number of highly polymorphic

compounds continues to grow, and soon compounds with five ambient polymorphs will no longer be considered unusual.

■ EXPERIMENTAL SECTION

Materials. Chemicals listed in Scheme 1 were purchased from Sigma-Aldrich expect ROY, which was purchased from TCI America. Purity provided by the manufacturer is as follows: oxalyl dihydrazide 98%, nicotinamide 99.5%, isonicotinamide 99%, coumarin 99%, paracetamol 98%, acridine 97%, theophylline 99%, carbamazepine 98%, dantron 96%, sulfapyridine 99%, imidacloprid 98%, ROY 97%, tolfenamic acid 98%, tolbutamide 97%, chlorpropamide 97%, flufenamic acid 97%, galunisertib 98%, aripiprazole 98%, and TES-ADT 99%. No purity information was provided for sulfathiazole and sulfameter. All chemicals were used without any purification. Initial polymorphs from chemicals are shown in Table 3. Controlled pore glass (CPG), a borate-silicate composite glass from which the borate phase is leached to produce a silica glass bead with a random pore network, was obtained from Biosearch Technologies (Petaluma, CA) with nominal pore sizes of 35 and 100 nm. Porous glass with nominal pore sizes of 8 nm were purchased from Sigma-Aldrich. All porous glasses were washed with nitric acid prior to use and then washed with deionized water and dried for 12 h under a vacuum. The acid-washed matrices were stored under air in a desiccator.

Melt Crystallization. Several milligrams of each compound were sandwiched between a 1 mm thick glass slide and a 0.1 mm glass coverslip or between two 0.1 mm glass coverslips and then melted to form a thin film. The thickness of these films ranged from 1 to $10~\mu m$. The melts were crystallized using a hot stage (Model FP90, Mettler-Toledo), a Kofler bench, or by rapid cooling between two metal blocks. Collectively, these platforms permitted crystallization over a

Table 1. Highly Polymorphic^a Compounds Not Studied in This Publication

| Material | NT | ref |
|--|----------------|-----|
| | $N_{ m total}$ | |
| 5-allyl-5-(2-cyclopenten-1-yl)-barbituric acid | 5 | 11 |
| 5-allyl-5-phenylbarbituric acid | 6 | 11 |
| aprobarbital | 6 | 11 |
| axitinib | 5 | 29 |
| barbital | 6 | 11 |
| 4-chloro-1,2,3,5-dithiadiazolyl radical | 5 | 30 |
| chlorphenoxamine hydrochloride | 5 | 11 |
| cocoa butter triacylglycerols | 6 | 32 |
| dantrolene | 6 | 33 |
| dehydroaripiprazole | 5 | 34 |
| 2-((4-(3,4-dichlorophenethyl)phenyl)amino)benzoic acid (molecule XXIII, PD-0118057 in the CCDC sixth blind test) | 5 | 35 |
| 5,5-dipropylbarbituric acid | 7 | 11 |
| ethallobarbital | 6 | 11 |
| griseofulvin | 5 | 36 |
| heptabarbital | 8 | 11 |
| hexamidine diisethionate | 10 | 37 |
| indomethacin | 8 | 38, |
| | | 39 |
| isonicotinic acid-(E)-(1-phenylethylidene)hydrazine | 6 | 40 |
| lauralkonium chloride | 5 | 11 |
| methyl-p-hydroxybenzoate | 6 | 11 |
| nifedipine | 6 | 41 |
| phenazopyridine | 5 | 11 |
| phenobarbital | 11 | 11 |
| picryl bromide | 5 | 30 |
| piroxicam | 8 | 42 |
| propallylonal | 5 | 11 |
| progesterone | 5 | 11 |
| triacetone-triperoxide | 6 | 30 |
| vemurafenib | 5 | 43 |
| ^a Total number of ambient polymorphs $N_{\text{total}} \geq 5$. | | |

wide range of temperatures, between either room temperature (20-25 °C) or refrigerator temperature (4–8 °C) and the melting point, $T_{\rm m}$. In a typical crystallization experiment, the starting material was sandwiched between two glasses and heated ca. 20 $^{\circ}\text{C}$ above T_{m} . The sample was then rapidly (within a few seconds) cooled to the desired temperature and held isothermally to observe crystallization and possible phase transformations. To speed up phase transformations, the sample would subsequently be heated to a higher temperature; however, all crystallization and phase transformation events were observed under isothermal conditions. The compounds were crystallized without additives as well as in the presence of natural resins such as Canada balsam, gum mastic, or Damar gum (a.k.a., Dammar crystals), at loadings of 10-15 wt %. It was observed that crystallization of some compounds could be accelerated by cooling the melt with the coverslip removed. Crystallization and phase transformations were monitored using polarized light optical microscopes Olympus BX50 and BX53 equipped with digital cameras. Polymorph identification for all distinct crystal morphologies was performed using powder X-ray diffraction.

Maximum linear growth rates, $V_{\rm max}$ were determined for all materials by measuring linear growth rates, V, of the fastest growing polymorph in a wide range of growth temperatures. Growth rate was determined as the displacement of the growth front divided by the elapsed time. Due to experimental limitations, these measurements were approximate for V > 1 mm/s (the actual value of V could deviate from the measured one up to two times), while for the remaining experiments precision was better than 10%. Nucleation rates were estimated only for sulfapyridne polymorphs. Samples were rapidly

cooled to a specific temperature, and nucleation rates were calculated as the number of nuclei per area of the sample per crystallization time.

Crystallization under Confinement. CPG beads were mixed physically with bulk crystals of one of the compounds in Scheme 1 and then heated above the compound's melting point in the differential scanning calorimetry (DSC) instrument for approximately two minutes to allow for infiltration into the pores by capillary action. The mixtures then were allowed to cool to room temperature within the DSC. Crystallization during this cooling cycle was evident from the appearance of an exothermic peak for most of the compounds in Scheme 1. Compounds that did not exhibit an exotherm were crystallized by annealing for hours to several days at a constant temperature ranging from 25 to 100 °C, depending on the compound. Based on the pore volume specified by the commercial source, and the mass ratio of each compound and CPG used, 67–70% of the pores were infiltrated.

Differential Scanning Calorimetry. DSC was performed on a Pyris-1 differential scanning calorimeter (PerkinElmer Inc., Wellesley, Massachusetts). Materials and material—CPG mixtures were heated and cooled at a rate of 10 °C/min. An indium standard was used to calibrate the instrument, and nitrogen was used as the purge gas. The data were analyzed using the PerkinElmer software to extract glass transition temperatures, melting points, and heats of fusion.

X-ray Diffraction. Polymorphs were identified using a Bruker D8 Discover General Area Detector Diffraction System (GADDS) equipped with a VÅNTEC-2000 2D detector and $\text{Cu-K}\alpha$ source (λ = 1.54178 Å). The X-ray beam was monochromated with a graphite crystal and collimated with a 0.5 mm capillary collimator (MONO-CAP). X-ray powder diffraction patterns were collected from powder loaded into 0.8 mm Kapton capillaries in transmission mode or from as-grown crystalline films on glass slides in reflection mode.

RESULTS

Melt crystallization in bulk and under confinement is described below for each compound in Scheme 1 in alphabetical order, along with relevant literature data. Tables 2, 3, and 4 list the compounds according to their molecular weights. Polymorph nomenclature for each compound corresponds to assignments provided in the Cambridge Structural Database (CSD). If the assignment in the CSD was unclear or incomplete, the designations from the original publications were used. The numbers of spontaneously nucleating polymorphs as a function of temperature are shown in Figure 1. Polarized light micrographs are shown only for new polymorphs and, in some cases, where there are no published high-quality images. PXRD patterns are presented only for new or unidentified polymorphs.

polymorphs. **Acridine**. 44–46 Acridine formed four polymorphs from the melt. Below ca. 85 °C it crystallizes as coarse spherulites of form VIII, which below ca. 40 °C is accompanied by branched high-birefringent crystals of form II, low-birefringent coarse spherulites of form IV, and finer high-birefringent spherulites of form VII (Figure 2A,B). Crystallization from the melt was reported to generate form II, which converted to form VIII at 40 °C. 44 Under confinement, acridine crystallized exclusively as form II in the range 80–90 °C for all pore sizes.

Aripiprazole.⁴⁷ Aripiprazole produced only form **IV** from the melt (Figure 2C) in our experiments, although form **III** has been reported in the literature to crystallize exclusively from the melt.⁴⁸ In CPG, aripiprazole crystallized as form **IV** within 8 nm pores, but the PXRD patterns collected for larger pore sizes revealed peaks at 9.6° and 12.2° that do not correspond to any known aripiprazole polymorph. Of note, aripiprazole is unstable under ambient conditions, and the PXRD data may correspond to a decomposition product that formed because

Table 2. Selected Properties of the Compounds in Scheme 1^a

| # | material | formula | refcode | M _w , g∕mol | T _m , °C | T _g , °C | $T_{ m g}/T_{ m m}$ | ΔH_m , kJ/mol | MF | $V_{ m max}$, $\mu{ m m/s}$ | T_{max} °C | ${T_{\rm max} / \atop T_{\rm m}}$ |
|----|--------------------|--------------------------|---------|------------------------|---------------------|---------------------|---------------------|-----------------------|----|------------------------------|-----------------------|-----------------------------------|
| 1 | oxalyl dihydrazide | $C_2H_6N_4O_2$ | VIPKIO | 118.1 | 242 | n.d. | n.d. | n.d. | F | 2000 | 180 | 0.88 |
| 2 | nicotinamide | $C_6H_6N_2O$ | NICOAM | 122.12 | 129 | -8 | 0.66 | 23.9 ^b | SR | 741 ^b | 100 | 0.93 |
| 3 | isonicotinamide | $C_6H_6N_2O$ | EHOWIH | 122.12 | 157 | 11 | 0.66 | 23.1 ^b | SR | 8000 ^b | 110 | 0.89 |
| 4 | coumarin | $C_9H_6O_2$ | COUMAR | 146.14 | 70 | -57 | 0.63 | 18.4 ^c | R | 2500 | 35 | 0.90 |
| 5 | paracetamol | $C_8H_9NO_2$ | HXACAN | 151.16 | 169 | 25 ^d | 0.67 | 27.4 ^e | SR | 391 ^f | 131 | 0.91 |
| 6 | acridine | $C_{13}H_9N$ | ACRDIN | 179.13 | 109 | n.d. | n.d. | 18.7^{g} | R | 10000 | 70 | 0.90 |
| 7 | theophylline | $C_7H_8N_4O_2$ | BAPLOT | 180.17 | 275 | 94 ^e | 0.67 | 29.6 ^e | SR | 1000 | 230 | 0.92 |
| 8 | carbamazepine | $C_{15}H_{12}N_2O$ | CBMZPN | 236.27 | 193 | 50 | 0.69 | 25.5 ^e | F | 45 | 165 | 0.94 |
| 9 | dantron | $C_{14}H_8O_4$ | DHANQU | 240.21 | 193 | n.d. | n.d. | 20.8 | R | 20000 | 150 | 0.91 |
| 10 | sulfapyridine | $C_{11}H_{11}N_3O_2S$ | BEWKUJ | 249.29 | 192 | 60 | 0.72 | 36.5 | FT | 130 | 150 | 0.91 |
| 11 | sulfathiazole | $C_9H_9N_3O_2S_2$ | SUTHAZ | 255.31 | 201 | 66 | 0.72 | 28.7 | FT | 91 | 170 | 0.93 |
| 12 | imidacloprid | $C_9H_{10}ClN_5O_2$ | HANFOS | 255.66 | 143 | 15 ^h | 0.69 | 28.1 ^h | FT | 39 | 114 | 0.93 |
| 13 | ROY | $C_{12}H_9N_3O_2S$ | QAXMEH | 259.29 | 115 | -14^{i} | 0.69 | 27.2 ⁱ | FT | 158 ^j | 80 | 0.91 |
| 14 | tolfenamic acid | $C_{14}H_{12}CINO_2$ | KAXXAI | 261.71 | 215 | 63 ^e | 0.69 | 38.8 ^e | F | 2000 | 150 | 0.87 |
| 15 | tolbutamide | $C_{12}H_{18}N_2O_3S$ | ZZZPUS | 270.35 | 128 | 11 ^k | 0.71 | 26.2 ^e | F | 19.2 | 110 | 0.96 |
| 16 | chlorpropamide | $C_{10}H_{13}ClN_2O_3S$ | BEDMIG | 276.74 | 130 | 16 ^e | 0.72 | 27.4 ^e | F | 7.8 | 115 | 0.96 |
| 17 | sulfameter | $C_{11}H_{12}N_4O_3S$ | SAMPYM | 280.3 | 211 | 67 | 0.70 | 38.7 | FT | 180 | 170 | 0.92 |
| 18 | flufenamic acid | $C_{14}H_{10}F_3NO_2$ | FPAMCA | 281.23 | 135 | 17^e | 0.71 | 27.1 ^e | F | 140 | 110 | 0.94 |
| 19 | galunisertib | $C_{22}H_{19}N_5O$ | DORDUM | 369.43 | 248 | n.d. | n.d. | 43.3 ¹ | F | 6 | 200 | 0.91 |
| 20 | aripiprazole | $C_{23}H_{27}Cl_2N_3O_2$ | MELFIT | 448.39 | 149 | 34 ^m | 0.73 | 38.4 ⁿ | F | 1.5 | 120 | 0.93 |
| 21 | TES-ADT | $C_{34}H_{38}S_2Si_2$ | MAMPAS | 566.97 | 155 | 27° | 0.70 | 23.7 | F | 63 | 110 | 0.89 |

 $^aM_{\rm w}$ — molecular weight; $T_{\rm m}$ — melting point of polymorph with the highest melting point; $T_{\rm g}$ — glass transition temperature; $\Delta H_{\rm m}$ — heat of fusion; $V_{\rm max}$ — maximum growth rate; $T_{\rm max}$ — temperature at which $V_{\rm max}$ was observed; MF — molecular flexibility (R = rigid; SR = semirigid; F = 1 flexible; FT = flexible with tautomerism). Source of data borrowed from literature: b ref [31], c ref [90], e ref [91], f ref [14], g ref [44], h ref [22], i ref [64], i ref [66], k ref [92], i ref [63], n ref [93], n ref [48], o ref [76].

the material—CPG mixture was held at high temperatures for longer times to allow infiltration of the pores.

Carbamazepine. 49 Carbamazepine crystallized as four polymorphs from the melt. Polymorph I dominated, crystallizing as fine spherulites with first to second order interference colors (form I was originally obtained from the melt⁵⁰). Form III grew as branched crystals with high interference colors, form IV as coarser spherulites with slightly lower birefringence, and a new form denoted VI formed coarse spherulites (Figures 2D,E and 3B). All three minor forms crystallized at 120-140 °C, concomitant with form I. After multiple melting/crystallization cycles, IV crystallized over a much wider temperature range suggesting the presence of decomposition products which influenced the polymorphic outcome. Under confinement in CPG, the absence of an exotherm failed to indicate crystallization during cooling in the DSC. Form I was observed in 35 and 100 nm pores only after annealing the sample at 100 °C overnight. Annealing carbamazepine in 8 nm pores at this temperature did not result in crystallization, but after several days at room temperature, the PXRD data revealed several diffraction peaks that signaled formation of a crystalline phase. The 2θ values for these peaks overlapped with those observed for some known carbamazepine polymorphs. The 2D diffraction pattern exhibited rings that precluded the possibility of preferred orientation, as would be expected for crystals in the randomly oriented nanopores in CPG. The absence of a match of the peak intensity pattern with those of other forms is consistent with the crystallization of a new polymorph (Figure 3B).

Chlorpropamide.⁵¹ Chlorpropamide crystallized from the melt as only form β , which at elevated temperatures, converted to form α , in agreement with a previous report⁵² that also described a $\beta \to \alpha$ transformation after prolonged storage at room temperature, accompanied by formation of a small

amount of ε and an unknown phase with diffraction peaks at $2\theta \approx 8$ and 10° . Form β was evident in all CPG pore sizes from several diffraction peaks corresponding to this form; however, in 8 nm pores one additional weak maximum not matching the β polymorph was detected at 6.4°. The PXRD patterns in 35 and 100 nm pores contained peaks at positions that did not match to those of the α , β , γ , δ , and ε phases indicated in Figure 3C nor to ambient η^{53} and ζ (Martin Ward, private communication) or nonambient phases α^{II} (refcode BEDMIG17), β^{II} (refcode BEDMIG11), β^{III} (refcode BEDMIG12), and ε' (refcode BEDMIG07). The 2D diffraction patterns for the CPG-confined chlorpropamide crystals were consistent with the randomized orientations, as expected, and the peak intensity patterns suggested the presence of at least three new polymorphs, although the possibility of a decomposition product cannot be excluded.

Coumarin. Coumarin crystallization from the melt, as reported previously by our laboratory, ¹⁸ occurs with concomitant nucleation of forms **II** and **IV** as well as a minor form **V**. Polymorph **III** is generated as a transformation product from form **IV**, while all four metastable forms eventually convert to form **I.** Our laboratory also reported that coumarin crystallized as form **I** from its melt in CPG pores >55 nm²⁶ but as a mixture forms **I** and **IV** in smaller pores in both CPG and porous poly(cyclohexylethylene) (*p*-PCHE) monoliths.

Dantron. Dantron (1,8-dihydroxyanthraquinone)⁵⁴ crystallization from the melt produces only form 4, which, at room temperature, converts to form 3. Forms 3 and 4 are enantiotropically related, with form 4 more stable above 155 °C. Under confinement in CPG pores, crystallization occurred upon cooling in the DSC. Crystallization in 35 and 100 nm pores occurred above 170 °C and produced form 4 and a minor amount of 3, while in 8 nm pores, crystallization

Table 3. Polymorphic and Crystallization Behavior of the Compounds in Scheme 1^a

| # | material | initial form c | $T_{\mathrm{m}\nu\mathrm{min}}$ $^{\circ}\mathrm{C}$ | ΔG_{m} , kJ/mol | ζ | $N_{ m total}$ | $N_{ m solved}$ | $N_{ m melt}$ | $N_{ m melt	ext{-}SS}$ | $N_{ m melt	ext{-}only}$ | $N_{ m conf}$ | $N_{ m conf-only}$ |
|----|--------------------|---------------------------|--|----------------------------------|--------------------|----------------|-----------------|---------------|------------------------|--------------------------|---------------|--------------------|
| 1 | oxalyl dihydrazide | α | n.d. | n.d. | 1.67 | 6 | 5 | 4 | 4 | 1 | n.d. | n.d. |
| 2 | nicotinamide | I | 103 | 1.55 | 1.00* ^b | 9 | 9 | 8(7) | 9(8) | 6 | 1 | 0 |
| 3 | isonicotinamide | I | <148 | >0.48 | 1.20 | 6 | 6 | 2 | 3 | 0 | 1 | 0 |
| 4 | coumarin | I | 54 | 0.86 | 1.04 | 5 | 5 | 3 | 5 | 3 | 2 | 0 |
| 5 | paracetamol | I | 100 | 4.28 | $1.00*^{b}$ | 6 | 4 | 6 | 6 | 3 | 2 | 0 |
| 6 | acridine | III | <89 | 0.98 | 1.08 | 8 | 6 | 4 | 4 | 0 | 1 | 0 |
| 7 | theophylline | II | n.d. | n.d. | $0.8*^{b}$ | 6 | 3 | 2 | 2 | 0 | 1 | 0 |
| 8 | carbamazepine | III | <175 | 0.98 | 1.25 | 6 | 5 | 4 | 4 | 1 | 1(2) | 1(0) |
| 9 | dantron | 1 | n.d. | n.d. | 0.59 | 5 | 5 | 1 | 2 | 0 | 2 | 0 |
| 10 | sulfapyridine | III | 167 | 1.96 | 0.95 | 7 | 5 | 4 | 5 | 1 | 1 | 0 |
| 11 | sulfathiazole | III + IV | 173 | 1.70 | 1.25 | 5 | 5 | 2(1) | 2(1) | 0 | 1 | 0 |
| 12 | imidacloprid | I | 99 | 2.97 | 1.14 | 9 | 8 | 5 | 8 | 1 | 1 | 1 |
| 13 | ROY | OP | 62 | 3.72 | 0.93 | 13 | 12 | 7(6) | 8(7) | 2 | 2 | 0 |
| 14 | tolfenamic acid | I | 207 | 0.63 | 1.25 | 10 | 9 | 4 | 4 | 1 | 2 | 0 |
| 15 | tolbutamide | $\mathbf{I}^{\mathbf{L}}$ | 106 | 1.44 | 0.78 | 7 | 7 | 4(3) | 5(3) | 0 | 2(1) | 1(0) |
| 16 | chlorpropamide | α | n.d. | n.d. | 2.67 | 7^d | 7^d | 1 | 3(2) | 0 | 4(1) | 3(0) |
| 17 | sulfameter | III | <155 | 4.48 | 1.78* ^b | 6 or 7 | 4 | 4 | 4 | 2 or 3 | 1 | 0 |
| 18 | flufenamic acid | I | 105 | 2.00 | 1.31 | 9 | 8 | 5(3) | 6(5) | 0 | 2 | 0 |
| 19 | galunisertib | VI | 172 | 6.32 | 0.83 | 10 | 10 | 1 | 1 | 0 | n.d. | n.d. |
| 20 | aripiprazole | n.d. | 135 | 1.27 | 1.45 | 11 | 8 | 2(1) | 2(1) | 0 | 2(1) | 1(0) |
| 21 | TES-ADT | α | 123 | 1.77 | 1.00* ^b | 7 | 1 | 5 | 5 | 4 | 2 | 0 |
| | | | | | | | | | | | | |

 $^aT_{\rm m,min}$ — melting point of polymorph with the lowest reported melting point; $\Delta G_{\rm m} = (T_{\rm m} - T_{\rm m,min}) \Delta H_{\rm m}/T_{\rm m}$ — free energy difference between polymorphs with the highest and lowest melting points (see eq 1). $N_{\rm total}$ — total number of ambient polymorphs. $N_{\rm melt}$ — number of polymorphs nucleating from the melt; $N_{\rm solved}$ — number of polymorphs, for which crystal structures were solved. $N_{\rm melt-SS}$ — number of polymorph accessible through melt crystallization including post-growth solid state transformations. $N_{\rm melt-only}$ — number of polymorphs obtained only through nucleation in melt crystallization. Numbers in parentheses are numbers of polymorphs observed in this study. $N_{\rm conf}$ — number of polymorphs obtained in nanoporous CPG using melt loading method through nucleation. $N_{\rm conf-only}$ — number of polymorphs among $N_{\rm conf}$ not obtained by other crystallization techniques. Numbers in parentheses are numbers of unambiguously confirmed polymorphs excluding forms suggested by only several diffraction peaks. n.d. — data are not available. ζ — complexity parameter calculated from eq 4. b Values labeled with an asterisk (*): Not informative situations, when either >80% of all polymorphs crystallize from the melt and/or there is no Z' available for ≥50% of all melt crystallized polymorphs. c Initial polymorph from chemicals used in experiments. d One new form and crystal structures for two forms of chlorpropamide are reported by Martin Ward but not yet published.

occurred around 100 $^{\circ}$ C and produced form 3 with a minor amount of 4.

Flufenamic Acid. 30 Flufenamic acid has been reported to crystallize directly from the melt as forms I, II, III, IV, and VIII (named as I, II, III, IV, and V in the original publication, respectively).⁵⁵ Polymorph IX was reported to form in solid dispersions⁵⁶ with polyethylene glycol. Our investigation found only three polymorphs (I, IV, and VIII) directly crystallizing from the melt. Polymorph I crystallized above 100 °C as clear coarse spherulites, polymorph IV as opaque spherulites over a wider range of range of temperatures (these are banded above ca. 100 °C), and polymorph VIII as fine spherulites below ca. 80 °C (Figure 2F). Solid state transformations, IV \rightarrow III, IV \rightarrow I, III \rightarrow II, and VIII \rightarrow II, were observed at 80-110 °C. Forms VIII and IV crystallized around 42-45 °C when embedded in CPG with pore sizes d = 30-200 from the melt.⁵⁷ These forms eventually converted to forms I, II, and III, although the pathway depended on pore size. Crystallization was not observed in 8 nm pores.

Galunisertib. Galunisertib polymorphism was screened recently by many methods, including melt crystallization.⁶ It was found that only form **VI** nucleated from the melt. We confirmed this. Crystallization in confinement was not performed because galunisertib degraded when held at an elevated temperature for the several minutes needed for pore infiltration.

Imidacloprid. Imidacloprid polymorphism has been previously investigated by our laboratory.²² Five polymorphs

crystallized from the melt – I and IX below 80 °C, II below 60 °C, V at room temperature, and VIII at 85–90 °C. Form VI was generated in the melt by cross nucleation from III. Form IV was obtained by seeding an imidacloprid melt with clothianidin crystals. All forms, except VII and the most stable I, could be generated via solid state transformations from the least stable IX, which is the dominant form when crystallization is performed below 100 °C. Crystallization of the metastable form VII could only be achieved under confinement in CPG pores. This polymorph could grow in a bulk melt seeded with CPG beads containing VII, but it underwent rapid conversion to form II.

Isonicotinamide.^{58,59} Isonicotinamide form **II** is the dominant form when crystallized from the melt in the whole temperature range. It is accompanied by a minor amount of form **VI** when crystallized below 40 °C.³¹ Form **II**, which is stable around the melting point, is enantiotropically related to form **I**, which is more stable at room temperature. Therefore, form **II** is slowly converted to form **I** at room temperature. In CPG, form **II** is observed for all pore sizes.

Nicotinamide. Nicotinamide has been known to form numerous polymorphs from the melt since the 1940s, 60,61 and it has been investigated recently by our laboratory 31 and others. 62 Eight forms can nucleate from the melt around 60–90 °C. Forms I (or α) and IV (or δ) appear at lower temperatures, and above this range, only form I is observed. Form III (or γ) crystallizes during the transformation from IV. Form VII (or η) was not observed here, although it has been

Table 4. Polymorphic Outcomes of Crystallization from Bulk and CPG-Confined Melts at the Temperatures Indicated in Parentheses^a

| | material | polymorph $(T_{\sigma}, {}^{\circ}C)$ | | | | | | | | |
|----|-----------------|---------------------------------------|------------------------------|--------------------------------|---|--|--|--|--|--|
| # | | 8 nm | 35 nm | 100 nm | bulk melt ^b | | | | | |
| 2 | nicotinamide | IV (62) | IV (59) | IV (68) | $IV > VIII > I > VI \gg IX (55-70)$ | | | | | |
| 3 | isonicotinamide | II (74) | II (118) | II (121) | II (>40) | | | | | |
| 4 | coumarin | $I + IV^c$ | \mathbf{IV}^c | \mathbf{I}^c | $II \approx IV \gg V (<35)$ | | | | | |
| 5 | paracetamol | III (77) | III (82) | III (88) | III \gg I, VII, VIII, IX (70–90) | | | | | |
| 6 | acridine | II (86) | II (83) | II (91) | VIII (80) | | | | | |
| 7 | theophylline | II (240) | II (240) | II (250) | II (>100) | | | | | |
| 8 | carbamazepine | UP (RT) | $I(100^d)$ | $I(100^d)$ | I (100) | | | | | |
| 9 | dantron | $3 \gg 4 (97)$ | $4 \gg 3 \ (174)$ | $4 \gg 3 \ (184)$ | 4 (all <i>T</i>) | | | | | |
| 10 | sulfapyridine | VII (90 ^d) | VII (90 ^d) | VII (90 ^d) | VII > V > IV (90) | | | | | |
| 11 | sulfathiazole | $I(100^d)$ | $I(100^d)$ | $I(100^d)$ | I (all <i>T</i>) | | | | | |
| 12 | imidacloprid | VII (RT) | VII (RT) | VII (RT) | $IX \gg I > II, V, VIII (RT)$ | | | | | |
| 13 | ROY | R (RT) | R (RT) | Y (RT) | $YN > R > ON \gg Y04, R05, Y (RT)$ | | | | | |
| 14 | tolfenamic acid | X (122) | V (138) | V (111) | $IV \approx V (>100)$ | | | | | |
| 15 | tolbutamide | UP (RT) | V (RT) | V (RT) | $V \gg II (<80)$ | | | | | |
| 16 | chlorpropamide | β + UP (RT) | β + UP (RT) | β + UP (RT) | β (RT) | | | | | |
| 17 | sulfameter | NC | NC | $V(115^d)$ | $\mathbf{V} \approx \mathbf{VI} \gg \mathbf{VII}, \mathbf{III} (115)$ | | | | | |
| 18 | flufenamic acid | NC | VIII > IV (46) | VIII > IV (44) | IV > VIII (<80) | | | | | |
| 20 | aripiprazole | IV (RT) | UP (RT) | UP (RT) | IV (all T) | | | | | |
| 21 | TES-ADT | γ (100) | $\gamma + \varepsilon$ (94) | $\gamma + \varepsilon$ (72,90) | $\gamma > \beta > \delta > \alpha $ (40–105) | | | | | |

"In cases for which more than one polymorph is observed, the relative amounts are reported. ^bPolymorphic outcomes for bulk melt are indicated only for comparison with crystallization in nanoconfinement for the similar temperature ranges. The complete list of polymorphs obtained from bulk melt is discussed in the text. ^cCrystallization temperature is not known; pore sizes were 7.8, 23, and 55 nm instead of 8, 35, and 100 nm (ref 24). ^dSample was cooled to room temperature and then annealed at given temperature. RT – crystallization at room temperature outside DSC. NC – no crystallization observed. UP - unidentified and possibly new polymorphs.

reported to crystallize from the melt at 60-80 °C.⁶² In CPG, only form **IV** was obtained for all pore sizes.

Oxalyl Dihydrazide. Oxalyl dihydrazide crystallizes rapidly from the melt, although it decomposes partially during melting with concomitant release of hydrazine. Needle-like crystals of form γ emerge rapidly above 150 °C when cooling from the melt. Below 60 °C, form γ forms spherulites. PXRD patterns of melt grown crystals at these temperatures are consistent with form γ , with additional reflections, some of which can be assigned to forms α and ε but others to a new polymorph, denoted here as ζ (Figure 3D). Crystallization in confinement was not performed because oxalyl dihydrazide would decompose during the time required for infiltration into the pores.

Paracetamol. Paracetamol (acetaminophen) crystallization from the melt has been investigated in considerable detail in our laboratory. All ambient forms can crystallize from the bulk melt, with major forms I and III and minor forms VII, VIII, and IX concomitantly nucleating above $T_{\rm g} \approx 25~{\rm ^{\circ}C}$. Only form II nucleates below $T_{\rm g}$. Previous reports have demonstrated crystallization of form III in CPG ($d=22-103~{\rm nm}$) at 80 °C accompanied by formation of form II in larger pore sizes. Polymorph conversion III \rightarrow II easily occurred above 100 °C, although this process required temperature cycling in smaller pore sizes. Form I was obtained when the external surfaces of CPG beads were covered with paracetamol. The investigation here found crystallization of form III for all pore sizes, however.

ROY. ROY (5-methyl-2-[(2-nitrophenyl) amino]-3-thiophenecabonitrile) was reported to crystallize a mixture of forms **Y**, **Y04**, **YT04**, **YN**, **ON**, **R**, and **R05** upon cooling a melt, ^{64–66}, ⁶⁷ which our results corroborated. ⁶⁸ Nucleation is very slow above 50 °C. Below 40 °C form **YN** is readily formed,

accompanied by Y04, R, R05, ON, and Y below 35 °C. At room temperature, Y04 transforms to YT04. In the literature form PO13 has been obtained from the melt below 60 °C as well as from seeding a melt with crystals of a ROY derivative, ⁶⁹ but this form was not observed in our investigation. Under confinement, ROY crystallized at room temperature after 1 day and formed polymorph R inside 8 and 35 nm pores and polymorph Y inside 100 nm pores. Previous studies of ROY embedded within poly(cyclohexylethylene) (p-PCHE) monoliths (d = 30 nm) indicated formation of polymorph Y after evaporation of an infiltrated pyridine solution of ROY. After excess material was removed from the external monolith surface, melting and recrystallization afforded polymorph \mathbb{R}^{28}

Sulfameter. Sulfameter (sulfamethoxydiazine, sulfametoxydiazine)12,70 primarily crystallizes from the melt as two polymorphs, denoted here as V and VI, which dominate above and below ca. 120 °C, respectively. Form V crystallizes as fine spherulites with homogeneous interference colors, while form VI appears as fine spherulites with fibers varying in interference colors that suggests twisting. Below 120 °C a small fraction of fine disorganized spherulites of an additional form can be detected, denoted here as VII but may correspond to forms I, II, or IV. Below 120 °C one can also detect low-birefringent coarse spherulites of stable form III, which also sometimes nucleates above 150 °C (Figure 2G,H). All forms convert to form III above 150 °C. Forms III, V, VI, and VII grown from the melt were previously assigned decades ago as I, II, III, and IV. 71 PXRD patterns of forms V and VI (Figure 3E) have not been reported. Of note, we were not able to collect a PXRD pattern of the very minor form VII. Early reports of sulfameter polymorphs did not contain PXRD data, and it is possible that two of the three forms V, VI, and VII observed here may correspond to two of the reported polymorphs earlier. The

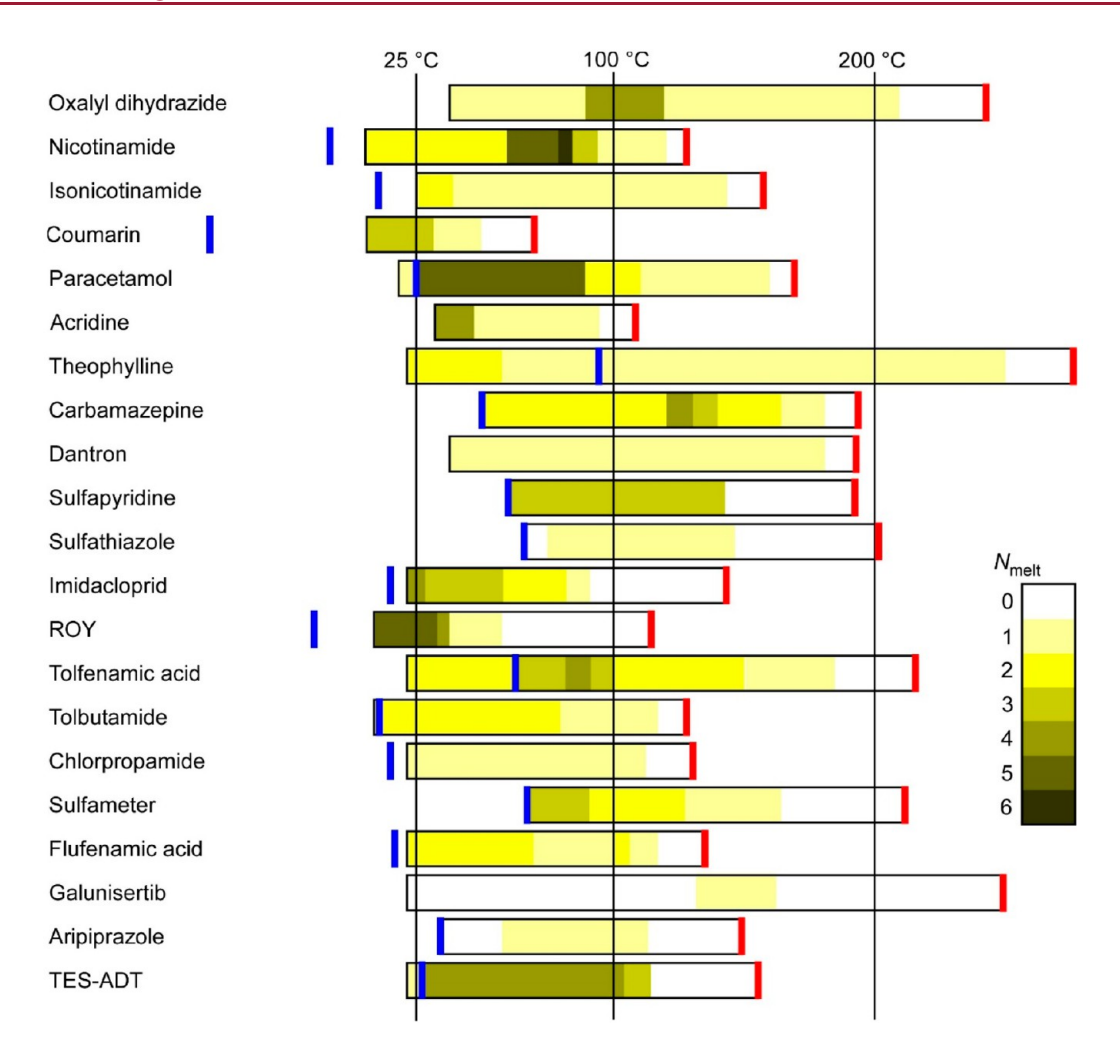


Figure 1. Number of polymorphs, $N_{\text{mel}\nu}$ that crystallize spontaneously from the melt over specified temperature ranges. The vertical red and blue bars correspond to the melting point of the polymorph with the highest T_{m} and to the glass transition temperature, respectively. $N_{\text{mel}\nu} = 0$ corresponds to the situation when no spontaneous nucleation was observed within at least one hour.

absence of crystal structure data for the previously reported forms precludes definitive assignment, but at least one of these must be new. Sulfameter resisted crystallization from the melt when embedded in CPG with pore sizes 8 and 35 nm, even after annealing. Form **V** was observed in 100 nm pores after annealing at 115 °C, however.

annealing at 115 °C, however. **Sulfapyridine.** 72–74 Sulfapyridine from the melt crystallizes as four polymorphs III, IV, V, and VII (Figure 2I,J; they were identified from the melt previously as I, IV, V, and VI, respectively 1. The polymorph denoted here as VII exhibits a PXRD pattern (Figure 3F) distinct from the five forms reported in the CSD. It is reasonable to suggest that this PXRD data does not correspond to the more stable form I, for which no crystal structure is reported. Polymorphs IV, V, and VII crystallize concomitantly at 80-130 °C as fine spherulites with low birefringence. Polymorphs V and VII have similar appearances and PXRD patterns, with VII being less stable and readily converting to V. Polymorph IV forms banded spherulites (polymorphs III and VII can form banded spherulites as well but banding is not pronounced). At higher temperatures, stable form III nucleates as spherulites with high interference colors. Above 130 °C polymorph II (assigned as III in ref 71) readily forms block-like crystals inside spherulites of form IV. When infiltrated into CPG beads, no crystallization

was observed after cooling in the DSC, and the samples were subsequently annealed at 90 $^{\circ}$ C overnight to produce form **VII** across all pore sizes.

Sulfathiazole.⁷⁵ Sulfathiazole in our hands crystallized only as form I from the melt, although two forms ($T_{\rm m}=202$ and 175 °C) have been reported.⁷¹ After melt-infiltrated CPG beads were cooled in the DSC, no crystallization was observed, and the samples were annealed at 100 °C overnight to produce form I across all pore sizes.

TES-ADT. TES-ADT (5,11-bis (triethylsilylethynyl)-anthradithiophene) polymorphism was reported in the literature but not studied in detail. He observed five polymorphs from the melt, two of which (δ and ε) were not previously reported (Figures 2K–M, 4A), and the remaining three corresponded to forms α , β , and likely γ . If the latter form is not γ (not clear due to insufficient published data), then the total number of forms from the melt increases to six. Our limited X-ray diffraction data suggest that most TES-ADT polymorphs exhibit disorder, packing similarities, and high Z numbers. Form ε crystallizes at room temperature below $T_{\rm g}$ = 27 °C. It is replaced by major polymorphs β , γ , and δ as well as minor polymorph α above room temperature and below ca. 105 °C, above which the most stable at room temperature

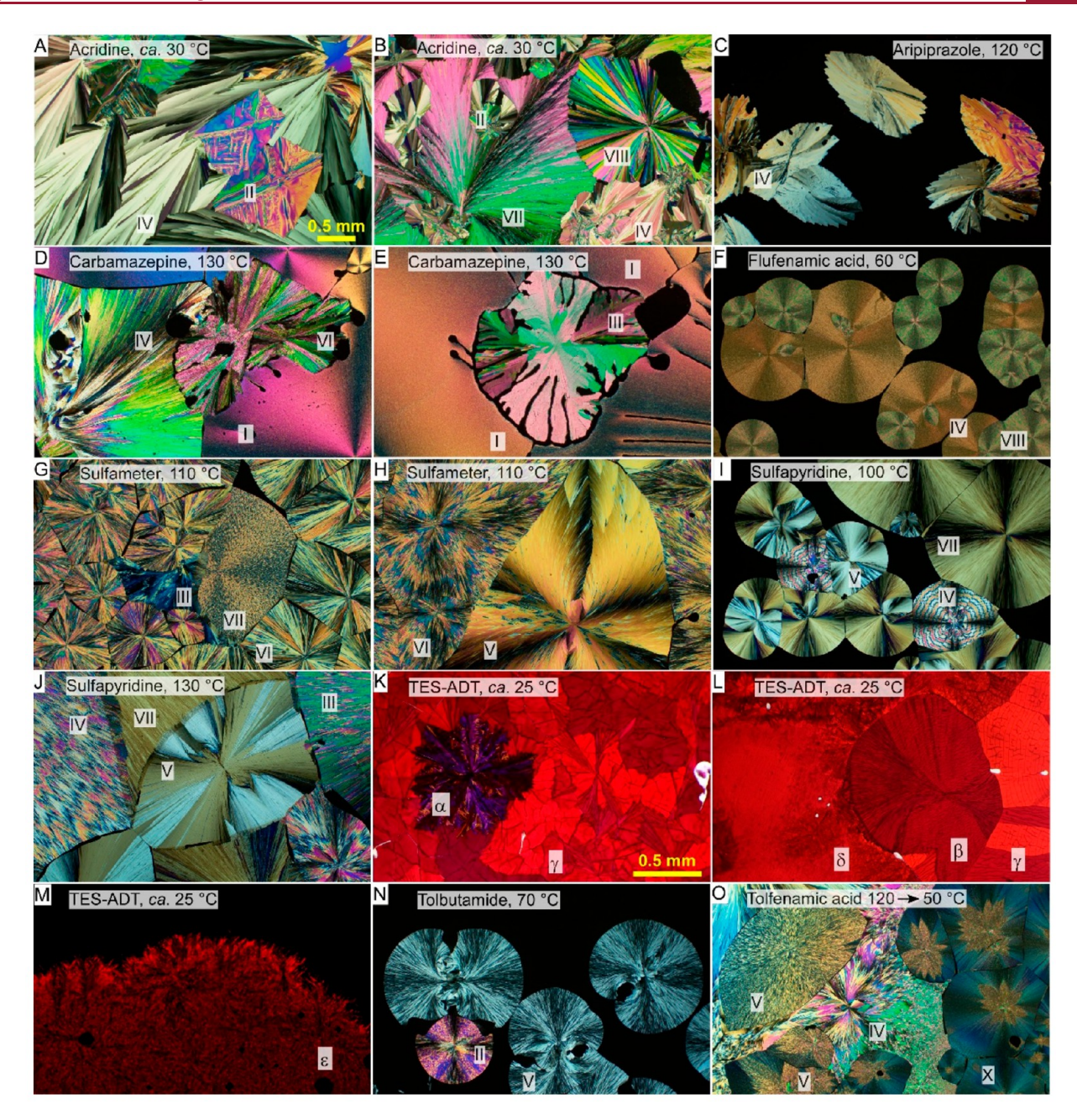


Figure 2. (A—O) Polarized light optical micrographs of selected compounds from Scheme 1. The scale bar in A is the same for all images except TES-ADT (K, L, M), for which the scale bar in panel K is used.

form α becomes less stable than polymorph β and stops nucleating. In confinement, only forms γ and ε were observed.

Theophylline. Theophylline crystallization from the melt is dominated by form $II^{79,80}$ with a minor amount of the rare and, based on similarities of PXRD patterns, likely structurally related form $V_{,}^{81}$ which typically crystallizes only near room temperature. Crystallization in confinement always resulted in form II.

Tolbutamide.^{82–84} Tolbutamide crystallization from the melt is dominated by coarse, low-birefringent spherulites of form **V**, accompanied by a small fraction of the more stable form **II** below ca. 80 °C, observed as finer spherulites with higher birefringence (Figure 2N). At elevated temperatures both forms convert to form **I**^L. Similar crystallization sequences were reported in the melt (forms **V**, **II**, and **I**^L were denoted

there as III, II, and I, respectively). Form IV also was reported to crystallize from the melt but was not observed in our experiments. Under confinement, crystallization was not observed during cooling inside the DCS. After sample storage at room temperature for 1 day, form V was detected in 35 and 100 nm pores, but crystallization was not observed in 8 nm pores. Form V also was obtained inside 3.2 nm pores of the MCM-41 host using a melt loading method. Above 60 °C, V \rightarrow IH transformation was observed. Annealing of tolbutamide infiltrated in 8 nm pore CPG only crystallized after standing for several days at room temperature. The PXRD pattern exhibited several peaks at 9.2°, 18.8°, 20.4°, and 21.8° (Figure 4B). The 2D diffraction patterns for the CPG-confined tolbutamide crystals were consistent with the absence of

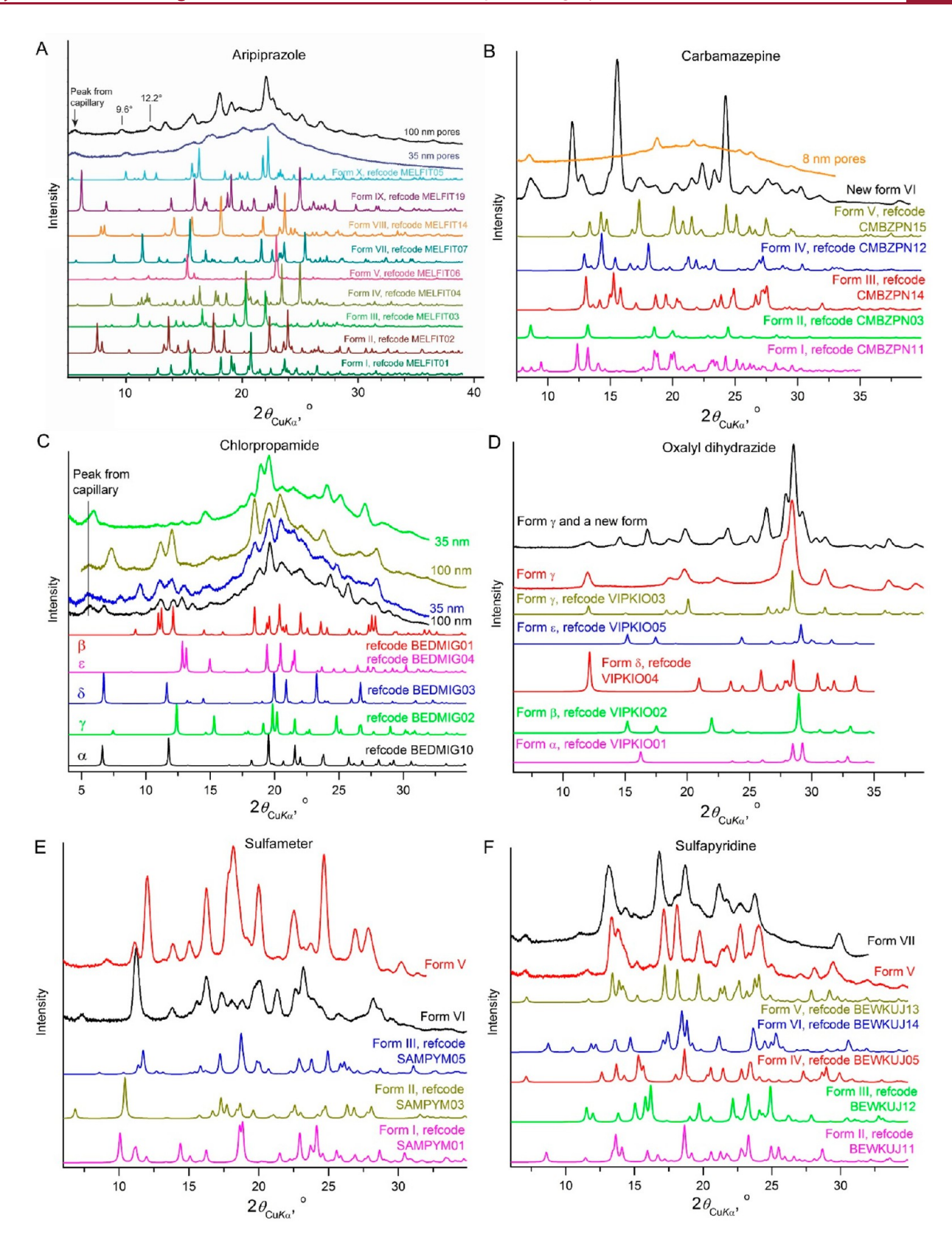


Figure 3. (A–F) PXRD patterns of new and unidentified polymorphs of the compounds in Scheme 1. Simulated PXRD patterns of known polymorphs with corresponding CSD refcodes are shown for comparison.

1

preferred orientation, as expected, and the peak intensity patterns suggested the presence of a new polymorph.

Tolfenamic Acid.^{86–89} Tolfenamic acid crystallizes from the melt as form **IV** (high-birefringent spherulites forming over the entire temperature range), form **V** (opaque spherulites

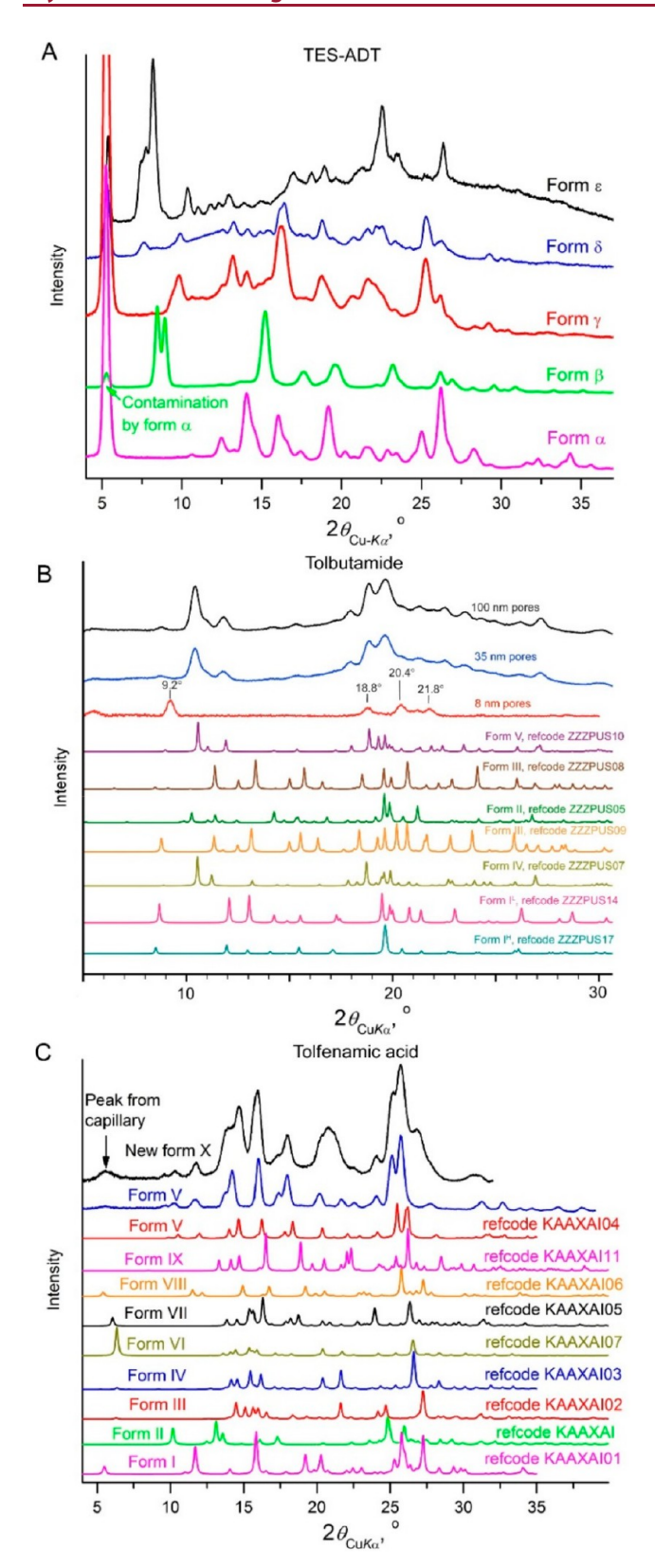


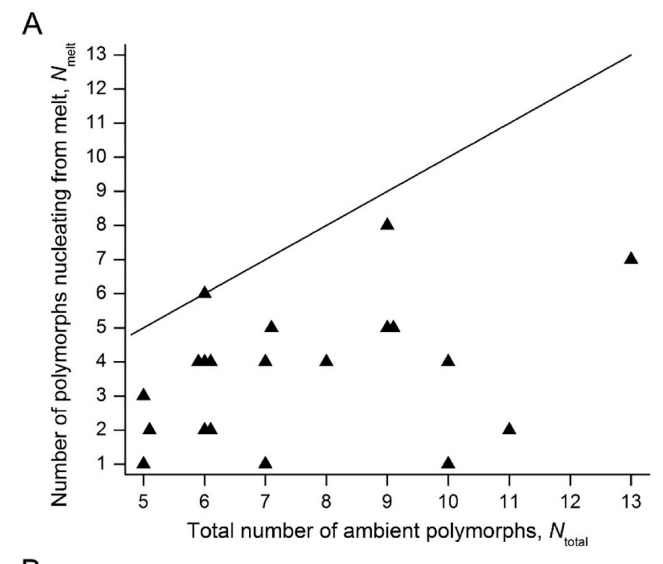
Figure 4. (A–C) PXRD patterns of new and unidentified polymorphs of the compounds in Scheme 1. Simulated PXRD patterns of known polymorphs with corresponding CSD refcodes are shown for comparison.

with first order interference colors crystallizing between 80–150 °C), form I (low-birefringent fine spherulites forming

between 65–90 °C that are evident only after several melt/crystallization cycles), and a new form provisionally called X (low-birefringent fine spherulites crystallizing below 100 °C). The PXRD pattern of form X closely resembles that of form V but has distinct signatures (Figures 2O and 4C). Polymorphs V and X form banded spherulites. At elevated temperature, all these forms convert to form I. Under confinement, crystallization occurred during sample cooling at 110–140 °C, producing form X in 8 nm pores and form V in larger pores.

DISCUSSION

Statistics of Bulk Melt Crystallization. The majority $(\geq 67\%)$ of all known forms can be obtained through direct nucleation from the melt for 6 of the 21 compounds in Scheme 1, while only one polymorph was observed for three compounds (Table 3, Figure 5A). When considering the



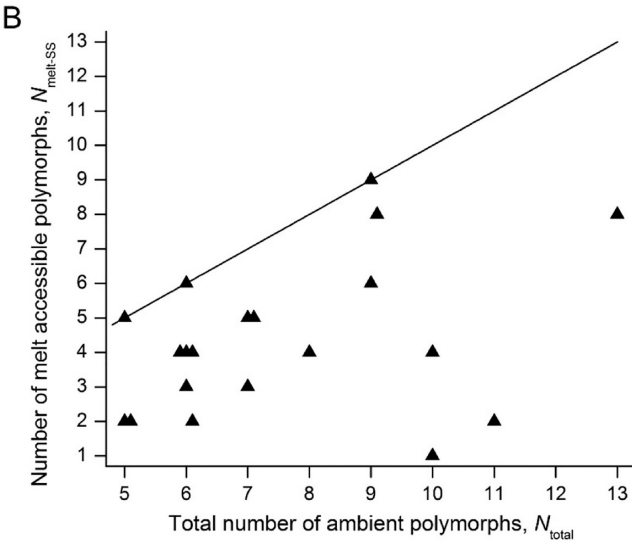


Figure 5. Number of polymorphs directly nucleating from the melt, $N_{\rm nucl}$ (A) and obtained from melt crystallization via nucleation and following solid-state transformations, $N_{\rm nucl-SS}$ (B) as a function of total number of ambient polymorphs, $N_{\rm total}$ for materials from Tables 2 and 3. The lines are intended to serve as a visual guide that corresponds to $N_{\rm nucl} = N_{\rm total}$ and $N_{\rm nucl-SS} = N_{\rm total}$, respectively.

practical goal of identifying all possible polymorphs, these numbers can be combined with the numbers of polymorphs obtained via solid state transformations following melt crystallization within experimentally reasonable time, here viewed as several weeks at room temperature or 2 days at elevated temperatures just below the melting point. This increases the number of compounds affording polymorphs from the melt—either directly or indirectly—to 11, while reducing the number of compounds forming only a single polymorph to one (Table 3, Figure 5B). On average, more than one-half of all ambient polymorphs can be revealed during melt crystallization, as given by eq 1, where $N_{\rm melt\text{-}SS}$ is number of polymorphs accessible through melt crystallization, including post-growth solid state transformations, and N_{total} is the number of known polymorphs for each compound.

$$\frac{1}{21} \sum_{i=1}^{21} \left(N_{\text{melt-SS}} / N_{\text{total}} \right)_i = 0.60$$
 (1)

Another important aspect concerns polymorphs obtained exclusively through melt crystallization. Twenty-five such polymorphs were identified for 11 of the 21 compounds in Scheme 1 and Table 3. Moreover, some of these polymorphs are crucial for obtaining new polymorphs via solid state transformations. Examples include polymorph IX -> III of imidacloprid,²² polymorph $IV \rightarrow III$ of coumarin,¹⁸ and polymorph $IV \rightarrow III$ of nicotinamide.⁶²

The percentage of accessible forms is not correlated with molecular weight, ostensible molecular rigidity, heat of fusion, or entropy of crystallization (Tables 2 and 3). Materials with similar molecular structures and thermochemistry can exhibit different numbers of polymorphs. For example, sulfathiozole and sulfapyridine, which have similar molecular structures (Scheme 1), molecular weight, heats of fusion, melting points, glass transition temperatures and growth rates, form similar numbers (five and seven, respectively) of ambient polymorphs. Polymorph I of sulfathiazole and polymorph VI of sulfapyridine have very similar lattice constants and packing motifs. Sulfathiazole, however, has only one polymorph by nucleation from the melt, while sulfapyridine has four. Nicotinamide forms eight of nine polymorphs by nucleation from the melt, while its regioisomer isonicotinamide forms only two of six.³¹ Inert additives such as Canada balsam and gum mastic have been reported to slow down crystallization and polymorph conversion, 14,17,18 but these additives did not alter the polymorphic outcomes described here.

Thermodynamic Driving Force. Metastable polymorphs have higher free energy and therefore require higher driving force for crystallization. During solution crystallization, high driving force is difficult to achieve because more stable polymorphs often crystallize more rapidly. Crystallization from the melt typically occurs between the melting point of the most stable form, $T_{\rm m}$, and the glass transition temperature, $T_{\rm g}$. The driving force for crystallization from the melt as a function of temperature T or supercooling $\Delta T = T_{\rm m} - T$ can be approximated as eq 2, ⁹⁴ where $\Delta H_{\rm m}$ is the heat of fusion.

$$\Delta G_{\rm V} = \frac{\Delta H_{\rm m} (T_{\rm m} - T)}{T_{\rm m}} \tag{2}$$

The approximation $T_{\rm g}=2T_{\rm m}/3^{94}$ (Table 2) translates to a maximum achievable driving force near $T_{\rm g}$ of $\Delta H_{\rm m}/3$, equivalent to 6-18 kJ/mol for the compounds in Table 2. This suggests that most polymorphs can be crystallized from

the melt given that 95% of polymorph pairs are described by lattice energy differences less than 7.2 kJ/mol.⁹⁵ The largest differences in polymorph melting points for the compounds in Scheme 1 are observed for galunisertib, paracetamol, and sulfameter, for which $(T_{\rm m}-T_{\rm m,min})$ = 76, 69, and 56 °C, respectively (Table 3). Supercooling can be easily achieved for these materials.

Kinetic Conditions. Growth rates from the melt are typically much less than growth rates from solution under comparable thermodynamic driving forces. In addition, the driving force for crystallization from the melt does not change until the entire melt is crystallized. These conditions favor detection of all nucleating polymorphs unlike some solution screening techniques, where the initially formed polymorph can rapidly consume all the material, leaving slow-crystallizing polymorphs undetected.

When a polymorph is thermodynamically accessible, nucleation, growth, and transformation kinetics determine if it will be detectable. Figure 6A shows a typical growth rate vs. temperature plot measured for sulfapyridine (similar plots are available for Table 2 compounds nicotinamide, 31,62 para-

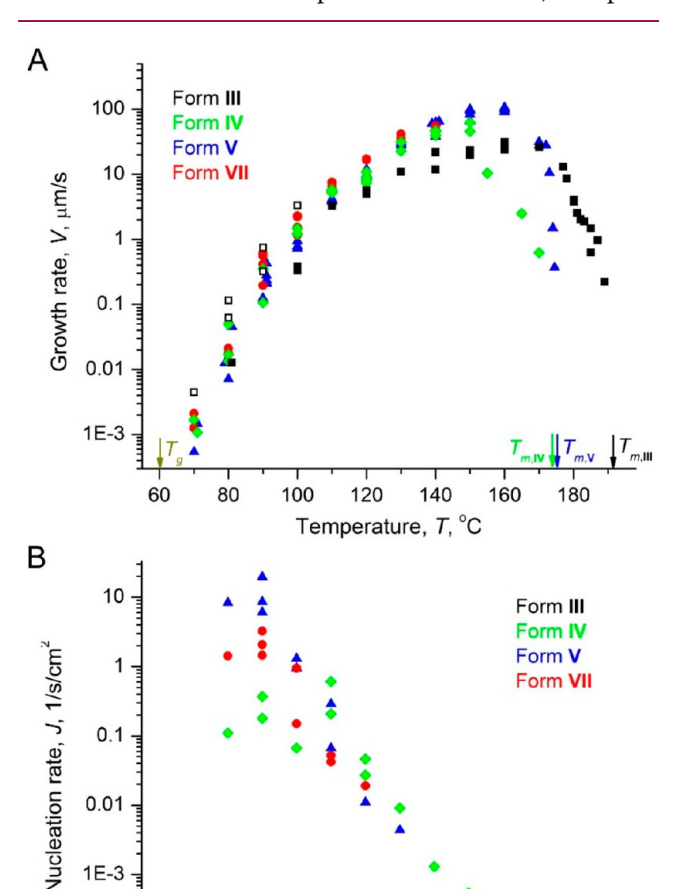


Figure 6. Dependence of the growth (A) and nucleation (B) rates of sulfapyridine polymorphs on temperature. Filled squares in (A) correspond to compact spherulites, whereas empty squares correspond to crystals with a fibrous morphology that may permit faster

120

Temperature, T, °C

140

160

1E-3

1E-4

60

80

100

cetamol, ¹⁴ and ROY⁶⁶). In the simplest approach, the effect of temperature on growth rate V(T) can be described by eq 3. ⁹⁶ The shape of the curve is determined by the competition between driving force for crystallization, which increases as temperature decreases (the second exponential term in eq 3), and the mobility of molecules in the melt, which increases as temperature increases (the first exponent in eq 3, which is roughly equivalent to the inverse viscosity of the melt). Here, V_0 is a constant that only slightly depends on temperature, R is the universal gas constant, and ΔG_D is an activation energy for the molecule in the melt to attach to the crystal.

$$V = V_0 \exp\left(-\frac{\Delta G_{\rm D}}{RT}\right) \left[1 - \exp\left(-\frac{\Delta G_{\rm V}}{RT}\right)\right]$$
(3)

The growth rate increases rapidly near the melting point, achieving its maximum value $V_{\rm max}$ at temperature $T_{\rm max}$, which corresponds to supercooling within the first tens of degrees $(T_{\rm max}/T_{\rm m}=0.87-0.96)$, see Table 2). At higher supercoolings, the driving force reaches a plateau, and growth rates begin to decrease due to the increased viscosity of the melt. Near the glass transition, the growth rates of all polymorphs become comparable, with differences rarely exceeding 1–1.5 orders of magnitude.

Figure 6B illustrates the dependence of a nucleation rate on temperature for sulfapyridine (a similar plot is available for nicotinamide³¹). According to classical nucleation theory,⁹⁴ the nucleation rate can be expressed by eq 4, where J_0 is a constant that is not strongly dependent on temperature, ΔG^* is the thermodynamic barrier for homogeneous nucleation, γ is the crystal-growth medium interface energy, and ω is the molar volume. In the case of heterogeneous nucleation, eq 4 remains valid when γ is adjusted for the substrate contribution. The shape of J(T) curve is determined by the competition between the driving force for crystallization (the second exponent in eq 4) and mobility of molecules in the melt (the first exponent in eq 4). The maximum nucleation rate occurs at lower temperatures than the maximum growth rate. Due to the strong temperature dependence of ΔG^* , nucleation can be slow for a wide range of temperatures about the melting and glass transition temperatures but remains measurable for intermediate temperatures.

$$J = J_0 \exp\left(-\frac{\Delta G_{\rm D} + \Delta G^*}{RT}\right)$$

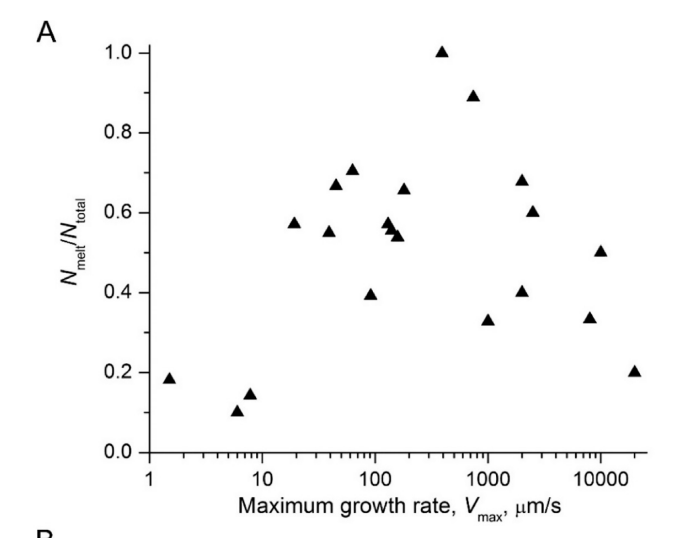
$$= J_0 \exp\left(-\frac{\Delta G_{\rm D}}{RT}\right) \exp\left(-\frac{16\pi}{3} \frac{\gamma^3 \omega^2}{RT \Delta G_{\rm V}^2}\right)$$
(4)

A small difference in γ or $\Delta G_{\rm V}$ can create a very large difference in nucleation rates at small supercoolings. As temperature decreases, nucleation rates become increasingly regulated by the molecular mobility, such that nucleation rates of different polymorphs become more similar.

Consequently, the largest number of polymorphs are more likely to be found when crystallization is performed slightly above $T_{\rm g}$, where the thermodynamic driving force is significant for all polymorphs, crystallization is relatively fast, and nucleation and growth are limited by molecular mobility. This is statistically confirmed for the compounds in Scheme 1. Two compounds do not crystallize close to $T_{\rm g}$, five compounds exhibit only one polymorph, and one compound forms the same number of polymorphs over the whole temperature

range. These eight compounds cannot inform the hypothesis being tested and were therefore excluded from consideration. Nine of the 13 remaining compounds form the maximum number of concomitantly crystallizing polymorphs at temperatures slightly above glass transition temperatures (Figure 1). Only four compounds form the maximum number of polymorphs below (one polymorph) or well above (three polymorphs) $T_{\rm g}$.

No correlation between maximum growth rate and the number of nucleating polymorphs was found (Figure 7A),



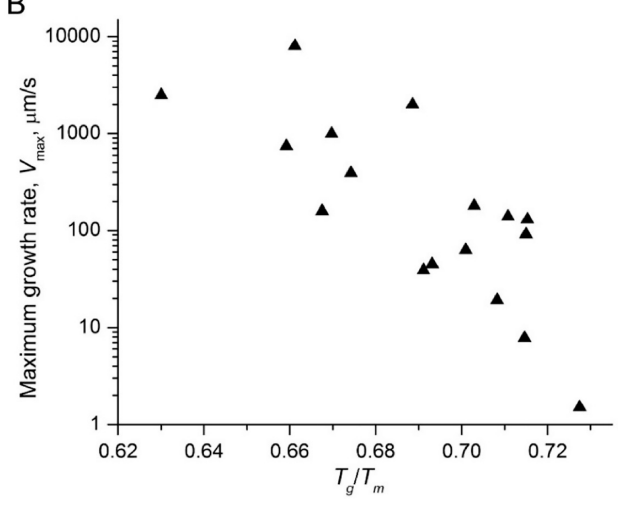


Figure 7. (A) Dependence of the number of crystallizing polymorphs $N_{\rm melt}/N_{\rm total}$ on maximum growth rate, $V_{\rm max}$. (B) Dependence of maximum growth rate, $V_{\rm max}$ on $T_{\rm g}/T_{\rm m}$.

although this may be attributed to the difficulty of finding multiple polymorphs at very high and very low growth rates. Indeed, sometimes the fastest growing polymorph still requires an inconveniently long time to be detected. If growth of a second polymorph is even 1 order of magnitude slower, the waiting time can become impractically long. Moreover, $V_{\rm max}$ typically corresponds to $T_{\rm max}/T_{\rm m}=0.87-0.96$ (Table 2), while as described above the best conditions for finding polymorphs is $T\approx T_{\rm g}\approx 0.7T_{\rm m}$, where the growth rate is significantly lower and detection of even the fastest-growing form becomes problematic. Aripiprazole and galunisertib, which are characterized by the smallest $V_{\rm max}$ and exhibit one polymorph each,

do not crystallize close to $T_{\rm g}$ (Figure 1). In the limit of very fast growth, the first crystal consumes most of the melt, before the next one nucleates, and even a slightly slower nucleating polymorph can remain undetected. The fastest growing material, dantron (Table 2), falls into this category. The maximum growth rate was found to correlate with $T_{\rm g}/T_{\rm m}$ ratio for silicates. Similar correlation was revealed for the compounds examined here (Figure 7B). It suggests that the intermediate values of $V_{\rm max}$, which correlate with detection of maximum number of polymorphs, correspond to the ratios $0.66 < T_{\rm g}/T_{\rm m} < 0.72$.

Crystal Structure Complexity. Crystal structure complexity is an intuitive, if not arbitrary, parameter that is not easily quantified. Nevertheless, we use a simple measure, ζ , which is defined for each compound in Scheme 1 as an average number of symmetry independent molecules (Z') in crystal structures of polymorphs directly nucleating from the melt, divided by the average Z' for all ambient polymorphs of the same compound (eq 5). This parameter becomes biased if most of the polymorphs can crystallize from the melt (e.g., nicotinamide) or if Z' is known for a small fraction of all and/or melt crystallized polymorphs (e.g., sulfameter provides at least four polymorphs from the melt but the crystal structure is known for only one of them). Such cases are marked with * in Table 3.

$$\zeta = \frac{N_{\text{total}} \sum_{i=1}^{N_{\text{melt}}} Z_i'}{N_{\text{melt}} \sum_{i=1}^{N_{\text{total}}} Z_i'}$$
(5)

Table 3 reveals that the melt-crystallized polymorphs are associated with higher complexity. For instance, only 4 of 21 compounds in Table 3 have ζ < 0.9, while 10 compounds have $\zeta > 1.1$, and for the rest $\zeta \approx 1$. When the probability of encountering various forms from the melt is taken into account, the prevalence of high Z' structures becomes even more vivid. For example, carbamazepine produces four forms from the melt, but the majority of crystals corresponds to form I with Z' = 4, while all other known polymorphs have Z' = 1. Likewise, imidacloprid forms five polymorphs from the melt with the dominating form IX having the highest Z' = 4. Even though the crystal structures of the TES-ADT polymorphs β , γ , and δ that dominate melt crystallization are not known, our preliminary X-ray diffraction study suggests that $Z' \ge 1$, 4, and 4, respectively, while Z' = 1 for the α polymorph that crystallizes from solution.

The correlation between melt crystallization and high Z' also can be deduced by calculating the percentage of different Z' values. In a study published in 2016, the fraction of high Z' structures among 274,315 organic compounds registered in the CSD was found to be very low with only 12.1% of structures having Z' > 1 and 1.3% structures having Z' > 2. In the investigation of melt crystallization described here, among 56 polymorphs with known Z' values, 25 (45%) have Z' > 1, 11 (20%) have Z' > 2, and 7 (13%) have Z' > 3. The prevalence of high Z' structures in melt crystallization was noted previously in a statistical analysis of 83 melt-crystallized polymorphs registered in the CSD, wherein Z' > 1 for 15 structures (18%), Z' > 2 for six (7%), and Z' > 3 for three (3.6%).

A statistical analysis of the CSD revealed that the percentage of structures with $Z^\prime > 1$ was larger for polymorphic compounds (ca. 20%) than monomorphic compounds (ca. 10%). Among 132 crystal structures available for 21

compounds Z' = 0.5, 1, 2, 3, and 4 were observed for 5, 77, 33, 6, and 8 structures, respectively, and three structures were reported to have Z' = 6, 9.5, and 20. Consequently, Z' > 1 for 38% of the 132 structures, Z' > 2 for 13%, and Z' > 3 for 8%. In comparison, only one of the 21 compounds in Scheme 1 (oxalyl dihydrazide) does not have Z' > 1.

We do not believe that the difference in complexity is related to the melt environment per se. Rather, melt crystallization more often produces high energy metastable polymorphs, which tend to have more complex organization. Finding high Z' polymorphs remains a significant challenge for the pharmaceutical industry because current crystal structure prediction methods (CSP) become computationally expensive for Z' > 1. For example, the frontline antitubercular drug isoniazid was considered to be monomorphic despite thorough screening. A CSP search limited to Z' = 1 and 2 initially predicted a significant energy gap (>6.5 kJ/mol) between the most stable form (later designated as form I) and the next lowest energy structure, which is typically viewed as characteristic of monomorphism.⁹⁵ Melt crystallization performed in our laboratory, however, led to the discovery of two additional polymorphs. The crystal structure of one of these new polymorphs, designated as form II, was solved as Z' = 4, which would not have appeared in the aforementioned CSP search.²¹ Following this observation, lattice energy calculations were performed, which revealed the energy of form II to be 5.5 kJ/mol greater than form L.103 The structure of highly metastable form III was not solved due to the absence of suitable single crystals and insufficient PXRD data, but it was found among the high-energy Z' = 1 CSP structures, 6.5 kJ/ mol above form I. This illustrates the utility of melt crystallization, which is predisposed to finding more polymorphs, as a companion to CSP searches.

Some compounds in Table 3 form polytypic structures or structures that are very similar, but most polymorphs have unique structure motifs. Out of 21 compounds in Scheme 1, six form polytypic or closely structurally related structures. Three compounds (dantron, sulfathiazole, and tolbutamide) form families of polytypic structures, but corresponding polymorphs do not crystallize from the melt. Three remaining compounds (theophylline, tolfenamic acid, and TES-ADT) identified here based only on the similarity of their PXRD patterns crystallize from the melt as families of closely structurally related polymorphs. Thus, no clear connection between formation of polytypic or very similar structures and melt crystallization can be established for this set of compounds.

Crystallization in Nanopores. Nineteen of the 21 compounds in Scheme 1 were embedded in CPG pores from their respective melts. Oxalyl dihydrazide and galunisertib (Tables 3, 4) were excluded because of their poor thermal stability. Crystallization in a range of pore sizes (8–100 nm) typically afforded only one or two polymorphs of those observed by crystallization from the bulk melt. Chlorpropamide was an exception, forming as many as four polymorphs within the nanopores. PXRD patterns acquired for 5 of the 19 compounds in the nanopores, however, contained peaks that were not consistent any known polymorph, suggesting new forms. Unambiguous identification of a new polymorph so far was obtained only for imidacloprid.

Seven of the 19 compounds crystallized under confinement in CPG pores produced only the phase that dominated crystallization from bulk melt at similar growth temperatures (Table 4). Another nine compounds produced the same outcome as the bulk melt along with the appearance of another polymorph, either exclusively in pores of specific sizes or in a mixture with the dominant polymorph. Only three of the compounds led to an entirely different outcome for all pore sizes than observed for bulk melt crystallization.

The observation of higher polymorph selectivity during crystallization under confinement can be attributed to various factors:

- One consequence of confinement is melting point depression, which is associated with a reduction in the total volume free energy ($\Delta G_{\rm V}$) of the nanometer-sized crystals. The melting point depression observed in 100 nm pores is typically only a few degrees, signaling a small difference between $\Delta G_{\rm V}$ of the confined and bulk crystals, which in turn would not be sufficient to significantly alter phase equilibria and crystallization significantly. Melting point depression in 8 nm pores, however, can approach several tens of degrees, indicating a large difference in $\Delta G_{\rm V}$ compared with the bulk, which can have a profound effect on the crystallization outcome.
- The small size of crystals confined in nanopores would be expected to reduce the likelihood of cross nucleation, thereby reducing the number of observable polymorphs.
- Detection of minor amounts of polymorphs during crystallization in nanopores is more challenging. PXRD and DSC typically can detect a second polymorph if its fraction of the sample is x > 0.01. Polarized optical microscopy, however, can detect a polymorph if x <10⁻⁵. For example, during paracetamol crystallization between 50 and 80 °C form III dominates, form I crystallizes often and primarily from the edges of the glass slide, form VII composes 3-5% of all crystals, form IX comprises <1%, and form VIII was observed only three times in ca. 400 samples. 14 This suggests that detection of form VII would be challenging for confined crystallization if its fraction resembled that observed in the bulk, and detection of forms VIII and IX would be highly unlikely. Indeed, only form III was observed for all pore sizes.

CONCLUSIONS

The results for crystallization of 21 highly polymorphic (at least 5 ambient polymorphs for each compound) materials from the bulk melts and melts in nanopores are summarized below.

- Crystallization from the melt is simple, fast, and inexpensive and can be applied to small sample sizes. It provides a facile approach to high driving force for crystallization with the potential to obtain all polymorphs. Accessible nucleation and transformation rates create opportunities for discovering highly metastable polymorphs.
- Melt crystallization affords, on average, half of all possible polymorphs, and in many cases (10 of 21 materials in this investigation) it reveals polymorphs not detected by other screening methods.
- There is a higher chance to discover a significant portion of all polymorphs using melt crystallization for materials exhibiting intermediate growth rates, $V_{\rm max} = 50-5000$ $\mu {\rm m/s}$, and intermediate $0.66 < T_{\rm g}/T_{\rm m} < 0.72$ ratios.

- On average, polymorphs obtained from the melt do not preferentially form polytypes and disordered structures, as sometimes claimed. Higher Z' values, which we view as reflecting more complex organization, are more common with melt crystallization. Consequently, crystallization from the melt is a useful tool to search for high Z' polymorphs that are not readily accessible by other experimental protocols and often overlooked by crystal structure prediction methods.
- Crystallization from melts embedded in nanopores results in one or two polymorphs, which typically are forms that dominate crystallization from the bulk melt at comparable temperatures. Polymorphs detected in nanopores represent either a subset of polymorphs obtained in the course of melt crystallization or new polymorphs not detected by any other crystallization technique (up to 5 of 19 materials in this study).

AUTHOR INFORMATION

Corresponding Author

Alexander G. Shtukenberg — Department of Chemistry and Molecular Design Institute, New York University, New York City, New York 10003, United States; ⊚ orcid.org/0000-0002-5590-4758; Email: shtukenberg@mail.ru

Authors

Noalle Fellah – Department of Chemistry and Molecular Design Institute, New York University, New York City, New York 10003, United States

Lamia Tahsin – Department of Chemistry and Molecular Design Institute, New York University, New York City, New York 10003, United States

Carolyn Jin Zhang — Department of Chemistry and Molecular Design Institute, New York University, New York City, New York 10003, United States

Bart Kahr — Department of Chemistry and Molecular Design Institute, New York University, New York City, New York 10003, United States; orcid.org/0000-0002-7005-4464

Michael D. Ward – Department of Chemistry and Molecular Design Institute, New York University, New York City, New York 10003, United States; orcid.org/0000-0002-2090-781X

Complete contact information is available at: https://pubs.acs.org/10.1021/acs.cgd.2c01065

Note:

The authors declare no competing financial interest.

ACKNOWLEDGMENTS

This work was supported by the National Science Foundation by DMREF Program under Award Number DMR-2118890, National Science Foundation Awards DMR-1708716 and DMR-2003968, and the National Science Foundation MRSEC Program under Award Number DMR-1420073. The X-ray microdiffractometer with GADDS was acquired through the support of the National Science Foundation under Award Number CRIF/CHE-0840277 and NSF MRSEC Program under Award Number DMR-0820341. The authors thank Prof. John H. Perepezko and Dr. Chengrong Cao (University of Wisconsin-Madison) for the glass transition temperature measurements of coumarin and isonicotinamide using their Mettler Toledo Flash DSC 2+ system. The authors thank Dr.

Martin Ward (University of Strathclyde, Glasgow) for the matching chlorpropamide powder diffraction pattern obtained for our samples crystallized in nanopores with the unpublished crystal structure of form ζ .

REFERENCES

- (1) Bernstein, J. *Polymorphism in Molecular Crystals*, 2nd ed.; Oxford University Press: Oxford, 2020.
- (2) Chung, H.; Diao, Y. Polymorphism as an emerging design strategy for high performance organic electronics. *J. Mater. Chem. C* **2016**, *4*, 3915–3933.
- (3) Bennion, J. C.; Matzger, A. Development and evolution of energetic cocrystals. J. Acc. Chem. Res. 2021, 54, 1699–1710.
- (4) Lee, A. Y.; Erdemir, D.; Myerson, A. S. Crystal polymorphism in chemical process development. *Annu. Rev. Chem. Biomol. Eng.* **2011**, *2*, 259–280.
- (5) Cruz-Cabeza, A. J.; Reutzel-Edens, S. M.; Bernstein, J. Facts and fictions about polymorphism. *Chem. Soc. Rev.* **2015**, *44*, 8619–8635.
- (6) Bhardwaj, R. M.; McMahon, J. A.; Nyman, J.; Price, L. S.; Konar, S.; Oswald, I. D. H.; Pulham, C. R.; Price, S. L.; Reutzel-Edens, S. M. A Prolific Solvate Former, Galunisertib, under the Pressure of Crystal Structure Prediction, Produces Ten Diverse Polymorphs. *J. Am. Chem. Soc.* 2019, 141, 13887–13897.
- (7) Yao, X.; Henry, R. F.; Zhang, G. G. Z. Ritonavir Form III: A new polymorph after 24 years. *J. Pharm. Sci.* **2022**, DOI: 10.1016/j.xphs.2022.09.026.
- (8) Lehmann, O. Die Krystallanalyse oder die chemische Analyse durch Beobachtung der Krystallbildung mit Hülfe des Mikroskops; Wilhelm Engelmann: Leipzig, 1891.
- (9) Kofler, L.; Kofler, A. Thermomikromethoden; Verlag Chemie: Weinheim, 1954.
- (10) McCrone, W. C. Fusion Methods in Chemical Microscopy; Interscience Publishers: New York, 1957.
- (11) Kuhnert-Brandstätter, M. Thermomicroscopy in the Analysis of Pharmaceuticals; Pergamon Press: Oxford, 1971.
- (12) Burger, A.; Ramberger, R. On the polymorphism of pharmaceuticals and other molecular crystals. II applicability of thermodynamic rules. *Mikrochim. Acta* 1979, 72, 273–316.
- (13) Ou, X.; Li, X.; Rong, H.; Yu, L.; Lu, M. A general method for cultivating single crystals from melt microdroplets. *Chem. Commun.* **2020**, *56*, 9950–9953.
- (14) Shtukenberg, A. G.; Tan, M.; Vogt-Maranto, L.; Chan, E. J.; Xu, W.; Yang, J.; Tuckerman, M. E.; Hu, C. T.; Kahr, B. Melt crystallization for paracetamol polymorphism. *Cryst. Growth Des.* **2019**, *19*, 4070–4080.
- (15) Shtukenberg, A.; Freundenthal, J.; Gunn, E.; Yu, L.; Kahr, B. Glass-crystal growth mode for testosterone propionate. *Cryst. Growth Des.* **2011**, *11*, 4458–4462.
- (16) Zhu, Q.; Shtukenberg, A. G.; Carter, D. J.; Yu, T.-Q.; Yang, J.; Chen, M.; Raiteri, P.; Oganov, A. R.; Pokroy, B.; Polishchuk, I.; Bygrave, P. J.; Day, G. M.; Rohl, A. L.; Tuckerman, M. E.; Kahr, B. Resorcinol crystallization from the melt: A new ambient phase and new "riddles. *J. Am. Chem. Soc.* 2016, 138, 4881–4889.
- (17) Shtukenberg, A. G.; Hu, C. T.; Zhu, Q.; Schmidt, M. U.; Xu, W.; Tan, M.; Kahr, B. The third ambient aspirin polymorph. *Cryst. Growth Des.* **2017**, *17*, 3562–3566.
- (18) Shtukenberg, A. G.; Zhu, Q.; Carter, D. J.; Vogt, L.; Hoja, J.; Schneider, E.; Song, H.; Pokroy, B.; Polishchuk, I.; Tkatchenko, A.; Oganov, A. R.; Rohl, A. L.; Tuckerman, M. E.; Kahr, B. Powder diffraction and crystal structure prediction identify four new coumarin polymorphs. *Chem. Sci.* **2017**, *8*, 4926–4940.
- (19) Yang, J.; Hu, C. T.; Zhu, X.; Zhu, Q.; Ward, M. D.; Kahr, B. DDT Polymorphism and the lethality of crystal forms. *Angew. Chem.* 2017. 129. 10299–10303.
- (20) Fellah, N.; Shtukenberg, A. G.; Chan, E. J.; Vogt-Maranto, L.; Xu, W.; Li, C.; Tuckerman, M. E.; Kahr, B.; Ward, M. D. Disorderly conduct of benzamide IV: Crystallographic and computational

- analysis of high entropy polymorphs of small molecules. Cryst. Growth Des. 2020, 20, 2670-2682.
- (21) Zhang, K.; Fellah, N.; Shtukenberg, A. G.; Fu, X.; Hu, C.; Ward, M. D. Discovery of new polymorphs of the tuberculosis drug isoniazid. *CrystEngComm* **2020**, 22, 2705–2708.
- (22) Zhu, X.; Hu, C. T.; Erriah, B.; Vogt-Maranto, L.; Yang, J.; Yang, Y.; Qiu, M.; Fellah, N.; Tuckerman, M. E.; Ward, M. D.; Kahr, B. Imidacloprid crystal polymorphs for disease vector control and pollinator protection. *J. Am. Chem. Soc.* **2021**, *143*, 17144–17152.
- (23) Jiang, Q.; Ward, M. D. Crystallization under nanoscale confinement. *Chem. Soc. Rev.* **2014**, *43*, 2066–2079.
- (24) Hamilton, B. D.; Ha, J.-M.; Hillmyer, M. A.; Ward, M. D. Manipulating crystal growth and polymorphism by confinement in nanoscale crystallization chambers. *Acc. Chem. Res.* **2012**, *45*, 414–423
- (25) Meldrum, F. C.; O'Shaughnessy, C. Crystallization in confinement. *Adv. Mater.* **2020**, *32*, 2001068.
- (26) Ha, J.-M.; Hamilton, B. D.; Hillmyer, M. A.; Ward, M. D. Phase behavior and polymorphism of organic crystals confined within nanoscale chambers. *Cryst. Growth Des.* **2009**, *9*, 4766–4777.
- (27) Hamilton, B. D.; Hillmyer, M. A.; Ward, M. D. Glycine polymorphism in nanoscale crystallization chambers. *Cryst. Growth Des.* **2008**, *8*, 3368–3375.
- (28) Ha, J.-M.; Wolf, J. H.; Hillmyer, M. A.; Ward, M. D. Polymorph selectivity under nanoscopic confinement. *J. Am. Chem. Soc.* **2004**, 126, 3382–3383.
- (29) Cruz-Cabeza, A. J.; Bernstein, J. Conformational polymorphism. *Chem. Rev.* **2014**, *114*, 2170–2191.
- (30) López-Mejías, V.; Kampf, J. W.; Matzger, A. J. Nonamorphism in flufenamic acid and a new record for a polymorphic compound with solved structures. *J. Am. Chem. Soc.* **2012**, *134*, 9872–9875.
- (31) Fellah, N.; Zhang, C. J.; Chen, C.; Hu, C. T.; Kahr, B.; Ward, M. D.; Shtukenberg, A. G. Highly polymorphous nicotinamide and isonicotinamide: Solution versus melt crystallization. *Cryst. Growth Des.* **2021**, *21*, 4713–4724.
- (32) Ghazani, S. M.; Marangoni, A. G. Molecular origins of polymorphism in cocoa butter. *Annu. Rev. Food Sci. Technol.* **2021**, *12*, 567–590.
- (33) Kons, A.; Mishnev, A.; Mukhametzyanov, T. A.; Buzyurov, A. V.; Lapuk, S. E.; Bérziņš, A. Hexamorphism of dantrolene: insight into the crystal structures, stability, and phase transformations. *Cryst. Growth Des.* **2021**, *21*, 1190–1201.
- (34) Zeidan, T. A.; Trotta, J. T.; Chiarella, R. A.; Oliveira, M. A.; Hickey, M. B.; Almarsson, Ö.; Remenar, J. F. Polymorphism of dehydro-aripiprazole, the active metabolite of the antipsychotic drug aripiprazole (abilify). *Cryst. Growth Des.* **2013**, *13*, 2036–2046.
- (35) Samas, B.; Clark, W. D.; Li, A.-F.; Pickard, F. C. IV; Wood, G. P. F. Five degrees of separation: Characterization and temperature stability profiles for the polymorphs of PD-0118057 (Molecule XXIII). *Cryst. Growth Des.* **2021**, 21, 4435–4444.
- (36) Ou, X.; Li, S.; Chen, Y.; Rong, H.; Li, A.; Lu, M. Polymorphism in griseofulvin: New story of an old drug with polyethylene glycol. *Cryst. Growth Des.* **2022**, 22, 3778–3785.
- (37) Edkins, K.; McIntyre, G. J.; Wilkinson, C.; Kahlenberg, V.; Többens, D.; Griesser, U. J.; Brüning, J.; Schmidt, M. U.; Steed, J. W. Extensive sequential polymorphic interconversion in the solid state: Two hydrates and ten anhydrous phases of hexamidine diisethionate. *Cryst. Growth Des.* **2019**, *19*, 7280–7289.
- (38) Surwase, S. A.; Boetker, J. P.; Saville, D.; Boyd, B. J.; Gordon, K. C.; Peltonen, L.; Strachan, C. J. Indomethacin: new polymorphs of an old drug. *Mol. Pharmaceutics* **2013**, *10*, 4472–4480.
- (39) Lightowler, M.; Li, S.; Ou, X.; Zou, X.; Lu, M.; Xu, H. Indomethacin Polymorph δ Revealed To Be Two Plastically Bendable Crystal Forms by 3D Electron Diffraction: Correcting a 47-Year-Old Misunderstanding. *Angew. Chem., Int. Ed.* **2022**, *61*, No. e202114985.
- (40) Hean, D.; Gelbrich, T.; Griesser, U. J.; Michael, J. P.; Lemmerer, A. Structural insights into the hexamorphic system of an isoniazid derivative. *CrystEngComm* **2015**, *17*, 5143–5153.

- (41) Gui, Y.; Jin, Y.; Ruan, S.; Sun, G.; López-Mejías, V.; Yu, L. Crystal energy landscape of nifedipine by experiment and computer prediction. *Cryst. Growth Des.* **2022**, *22*, 1365–1370.
- (42) Yao, C.; Guzei, I. A.; Jin, Y.; Ruan, S.; Sun, G.; Gui, Y.; Wang, L.; Yu, L. Polymorphism of piroxicam: new polymorphs by melt crystallization and crystal structure prediction. *Cryst. Growth Des.* **2020**, *20*, 7874.
- (43) Li, S.; Lightowler, M.; Ou, X.; Huang, S.; Jiang, Y.; Li, X.; Zou, X.; Xu, H.; Lu, M. Direct structure determination from spherulites using 3D electron diffraction. *ChemRxiv* Cambridge Open Engage: Cambridge, 2022, DOI: 10.26434/chemrxiv-2022-jh1lx.
- (44) Braga, D.; Grepioni, F.; Maini, L.; Mazzeo, P. P.; Rubini, K. Solvent-free preparation of co-crystals of phenazine and acridine with vanillin. *Thermochim. Acta* **2010**, *507*–*508*, 1–8.
- (45) Kupka, A.; Vasylyeva, V.; Hofmann, D. W. M.; Yusenko, K. V.; Merz, K. Solvent and isotopic effects on acridine and deuterated acridine polymorphism. *Cryst. Growth Des.* **2012**, *12*, 5966–5971.
- (46) Herbstein, F. H.; Schmidt, G. M. J. The crystal and molecular structures of heterocyclic compounds. I. the analysis of the crystal structure of α -phenazine. *Acta Crystallogr.* **1955**, *8*, 399–405.
- (47) Brittain, H. G. Aripiprazole: Polymorphs and solvatomorphs. In *Profiles of Drug Substances, Excipients, and Related Methodology*; Elsevier, 2012; Vol. 37, pp 1–29.
- (48) Braun, D. E.; Gelbrich, T.; Kahlenberg, V.; Tessadri, R.; Wieser, J.; Griesser, U. J. Conformational polymorphism in aripiprazole: Preparation, stability and structure of five modifications. *J. Pharm. Sci.* **2009**, *98*, 2010–2026.
- (49) Arlin, J.-B.; Price, L. S.; Price, S. L.; Florence, A. J. A strategy for producing predicted polymorphs: catemeric carbamazepine form V. *Chem. Commun.* **2011**, 47, 7074–7076.
- (50) Grzesiak, A. L.; Lang, M.; Kim, K.; Matzger, A. J. Comparison of the four anhydrous polymorphs of carbamazepine and the crystal structure of form I. *J. Pharm. Sci.* **2003**, *92*, 2260–2271.
- (51) Drebushchak, T. N.; Chesalov, Y. A.; Boldyreva, E. V. A conformational polymorphic transition in the high-temperature ε -form of chlorpropamide on cooling: a new ε' -form. *Acta Crystallogr.* **2009**, *B65*, 770–781.
- (52) Drebushchak, T. N.; Drebushchak, V. A. Structural similarity and similarity in thermal properties of the polymorphs: melting and crystallization from the melt of tolbutamide and chlorpropamide. *J. Therm. Anal. Calorim.* **2020**, *142*, 841–848.
- (53) Belenguer, A. M.; Cruz-Cabeza, A. J.; Lampronti, G. I.; Sanders, J. K. M. On the prevalence of smooth polymorphs at the nanoscale: implications for pharmaceuticals. *CrystEngComm* **2019**, *21*, 2203–2211.
- (54) Rohl, A. L.; Moret, M.; Kaminsky, W.; Claborn, K.; McKinnon, J. J.; Kahr, B. Hirshfeld surfaces identify inadequacies in computations of intermolecular interactions in crystals: pentamorphic 1,8-dihydroxyanthraquinone. *Cryst. Growth Des.* **2008**, *8*, 4517–4525.
- (55) Kuhnert-Brandstätter, M.; Borka, L.; Friedrich-Sander, G. Zur Polymorphie von Arzneimitteln: Flufenaminsäure und BL 191. *Arch. Pharm. Pharm. Med. Chem.* 1974, 307, 845–853.
- (56) Sanabria Ortiz, K.; Hernandez Espinell, J. R.; Ortiz Torres, D.; Lopez-Mejias, V.; Stelzer, T. Polymorphism in solid dispersions. *Cryst. Growth Des.* **2020**, 20, 713–722.
- (57) Zhang, K.; Fellah, N.; López-Mejías, V.; Ward, M. D. Polymorphic phase transformation pathways under nanoconfinement: flufenamic acid. *Cryst. Growth Des.* **2020**, *20*, 7098–7103.
- (58) Eccles, K. S.; Deasy, R. E.; Fabian, L.; Braun, D. E.; Maguire, A. R.; Lawrence, S. E. Expanding the crystal landscape of isonicotinamide: concomitant polymorphism and co-crystallisation. *CrystEng-Comm* **2011**, *13*, 6923–6925.
- (59) Vicatos, A. I.; Caira, M. R. A new polymorph of the common coformer isonicotinamide. *CrystEngComm* **2019**, *21*, 843–849.
- (60) Kofler, L.; Kofler, A. Über Molekülverbindungen des Nicotinsäureamids. Ber. Dtsch. Chem. Ges. 1943, 76, 718–722.
- (61) Kofler, A.; Kolšek, J. Beitrag zur mikroskopischen Identifizierung organischer Stoffe nach L. Kofler. V. *Microchim. Acta* **1971**, 59, 848–874.

- (62) Li, X.; Ou, X.; Wang, B.; Rong, H.; Wang, B.; Chang, C.; Shi, B.; Yu, L.; Lu, M. Nicotinamide: rich polymorphism in nicotinamide revealed by melt crystallization and crystal structure prediction. *Commun. Chem.* **2020**, *3*, 152.
- (63) Rengarajan, G. T.; Enke, D.; Steinhart, M.; Beiner, M. Size-dependent growth of polymorphs in nanopores and Ostwald's step rule of stages. *Phys. Chem. Chem. Phys.* **2011**, *13*, 21367–21374.
- (64) Yu, L. Polymorphism in molecular solids: an extraordinary system of red, orange, and yellow crystals. *Acc. Chem. Res.* **2010**, *43*, 1257–1266.
- (65) Chen, S.; Guzei, I. A.; Yu, L. New polymorphs of ROY and new record for coexisting polymorphs of solved structures. *J. Am. Chem. Soc.* 2005, 127, 9881–9885.
- (66) Chen, S. A.; Xi, H. M.; Yu, L. Cross-nucleation between ROY polymorphs. J. Am. Chem. Soc. 2005, 127, 17439–17444.
- (67) Li, X.; Ou, X.; Rong, H.; Huang, S.; Nyman, J.; Yu, L.; Lu, M. The twelfth solved structure of ROY: single crystals of Y04 grown from melt microdroplets. *Cryst. Growth Des.* **2020**, *20*, 7093.
- (68) Tan, M.; Shtukenberg, A. G.; Zhu, S. C.; Xu, W. Q.; Dooryhee, E.; Nichols, S. M.; Ward, M. D.; Kahr, B.; Zhu, Q. ROY revisited, again: the eighth solved structure. *Faraday Discuss.* **2018**, *211*, 477–491.
- (69) Lévesque, A.; Maris, T.; Wuest, J. D. ROY reclaims its crown: new ways to increase polymorphic diversity. *J. Am. Chem. Soc.* **2020**, 142, 11873–11883.
- (70) Tailor, S. M.; Patel, U. H. Hirshfeld surface analysis of sulfameter (polymorph III), sulfameter dioxane monosolvate and sulfameter tetrahydrofuran monosolvate, all at 296 K. *Acta Crystallogr.* **2015**, *C71*, 944–953.
- (71) Kuhnert-Brandstätter, M.; Wunsch, S. Polymorphie und Mischkristallbildung bei Sulfonamiden und verwandten Verbindungen. *Mikrochim. Acta* **1969**, *57*, 1297–1307.
- (72) Bar, I.; Bernstein, J. Conformational polymorphism VI: the crystal and molecular structures of form II, form III, and form V of 4-amino-N-2-pyridinylbenzenesulfonamide (sulfapyridine). *J. Pharm. Sci.* 1985, 74, 255–263.
- (73) Burger, A.; Schulte, K.; Ramberger, G. Aufklärung thermodynamischer Beziehungen zwischen fünf polymorphen Modifikationen von Sulfapyridin mittels DSC. *J. Therm. Anal.* **1980**, *19*, 475–484.
- (74) Gelbrich, T.; Threlfall, T. L.; Bingham, A. L.; Hursthouse, M. B. Polymorph VI of sulfapyridine: interpenetrating two- and three-dimensional hydrogen-bonded nets formed from two tautomeric forms. *Acta Crystallogr.* **2007**, *C*63, o323–o326.
- (75) Abu Bakar, M. R.; Nagy, Z. K.; Rielly, C. D.; Dann, S. E. Investigation of the riddle of sulfathiazole polymorphism. *Int. J. Pharm.* **2011**, *414*, 86–103.
- (76) Yu, L.; Li, X.; Pavlica, E.; Koch, F. P. V.; Portale, G.; da Silva, I.; Loth, M. A.; Anthony, J. E.; Smith, P.; Bratina, G.; Kjellander, B. K. C.; Bastiaansen, C. W. M.; Broer, D. J.; Gelinck, G. H.; Stingelin, N. Influence of solid-state microstructure on the electronic performance of 5,11-bis(triethylsilylethynyl) anthradithiophene. *Chem. Mater.* 2013, 25, 1823–1828.
- (77) Lee, S. S.; Loth, M. A.; Anthony, J. E.; Loo, Y.-L. Orientation-independent charge transport in single spherulites from solution-processed organic semiconductors. *J. Am. Chem. Soc.* **2012**, *134*, 5436–5439.
- (78) Chen, J.; Shao, M.; Xiao, K.; Rondinone, A. J.; Loo, Y.-L.; Kent, P. R. C.; Sumpter, B. G.; Li, D.; Keum, J. K.; Diemer, P. J.; Anthony, J. E.; Jurchescu, O. D.; Huang, J. Solvent-type-dependent polymorphism and charge transport in a long fused-ring organic semiconductor. *Nanoscale* **2014**, *6*, 449–456.
- (79) Fucke, K.; McIntyre, G. J.; Wilkinson, C.; Henry, M.; Howard, J. A. K.; Steed, J. W. New insights into an old molecule: interaction energies of theophylline crystal forms. *Cryst. Growth Des.* **2012**, *12*, 1395–1401.
- (80) Khamar, D.; Pritchard, R. G.; Bradshaw, I. J.; Hutcheon, G. A.; Seton, L. Polymorphs of anhydrous theophylline: stable form IV consists of dimer pairs and metastable form I consists of hydrogen-

bonded chains. Acta Crystallogr. C Cryst Struct Commun 2011, 67, o496-o499.

- (81) Roy, C.; Vrel, D.; Vega-González, A.; Jestin, P.; Laugier, S.; Subra-Paternault, P. Effect of CO_2 -antisolvent techniques on size distribution and crystal lattice of theophylline. *J. Supercrit. Fluids* **2011**, *57*, 267–277.
- (82) Thirunahari, S.; Aitipamula, S.; Chow, P. S.; Tan, R. B. H. Conformational polymorphism of tolbutamide: a structural, spectroscopic, and thermodynamic characterization of Burger's forms I–IV. *J. Pharm. Sci.* **2010**, *99*, 2975–2990.
- (83) Drebushchak, T. N.; Drebushchak, V. A.; Pankrushina, N. A.; Boldyreva, E. V. Single-crystal to single-crystal conformational polymorphic transformation in tolbutamide at 313 K. Relation to other polymorphic transformations in tolbutamide and chlorpropamide. *CrystEngComm* **2016**, *18*, 5736–5743.
- (84) Nath, N. K.; Nangia, A. Novel form V of tolbutamide and a high Z' crystal structure of form III. CrystEngComm 2011, 13, 47–51.
- (85) Nartowski, K. P.; Malhotra, D.; Hawarden, L. E.; Fábián, L.; Khimyak, Y. Z. Nanocrystallization of rare tolbutamide form V in mesoporous MCM-41 silica. *Mol. Pharmaceutics* **2018**, *15*, 4926–4932.
- (86) López-Mejías, V.; Kampf, J. W.; Matzger, A. J. Polymer-induced heteronucleation of tolfenamic acid: structural investigation of a pentamorph. *J. Am. Chem. Soc.* **2009**, *131*, 4554–4555.
- (87) Case, D. H.; Srirambhatla, V. K.; Guo, R.; Watson, R. E.; Price, L. S.; Polyzois, H.; Cockcroft, J. K.; Florence, A. J.; Tocher, D. A.; Price, S. L. Successful computationally directed templating of metastable pharmaceutical polymorphs. *Cryst. Growth Des.* **2018**, *18*, 5322–5331.
- (88) Ranjan, S.; Devarapalli, R.; Kundu, S.; Saha, S.; Deolka, S.; Vangala, V. R.; Reddy, C. M. Isomorphism: 'molecular similarity to crystal structure similarity' in multicomponent forms of analgesic drugs tolfenamic and mefenamic acid. *IUCrJ.* **2020**, *7*, 173–183.
- (89) Sacchi, P.; Reutzel-Edens, S. M.; Cruz-Cabeza, A. J. The unexpected discovery of the ninth polymorph of tolfenamic acid. *CrystEngComm* **2021**, *23*, 3636–3647.
- (90) Qi, S.; Avalle, P.; Saklatvala, R.; Craig, D. Q. M. An investigation into the effects of thermal history on the crystallisation behaviour of amorphous paracetamol. *Eur. J. Pharm. Biopharm.* **2008**, 69, 364–371.
- (91) Baird, J. A.; van Eerdenbrugh, B.; Taylor, L. S. A classification system to assess the crystallization tendency of organic molecules from undercooled melts. *J. Pharm. Sci.* **2010**, *99*, 3787–3806.
- (92) Fukuoka, E.; Makita, M.; Nakamura, Y. Glassy state of pharmaceuticals. V. Relaxation during cooling and heating of glass by differential scanning calorimetry. *Chem. Pharm. Bull.* **1991**, 39, 2087—2090.
- (93) Jamróz, W.; Kurek, M.; Łyszczarz, E.; Szafraniec, J.; Knapik-Kowalczuk, J.; Syrek, K.; Paluch, M.; Jachowicz, R. 3D printed orodispersible films with aripiprazole. *Int. J. Pharm.* **2017**, 533, 413–420.
- (94) Fokin, V. M.; Zanotto, E. D.; Yuritsyn, N. S.; Schmelzer, J. W. P. Homogeneous crystal nucleation in silicate glasses: A 40 years perspective. *J. Non-Crystalline Sol.* **2006**, 352, 2681–2714.
- (95) Nyman, J.; Day, G. M. Static and lattice vibrational energy differences between polymorphs. *CrystEngComm* **2015**, *17*, 5154–5165.
- (96) Kirkpatrick, R. J. Crystal growth from the melt: A review. Am. Mineral. 1975, 60, 798–814.
- (97) Fokin, V. M.; Nascimento, M. L. F.; Zanotto, E. D. Correlation between maximum crystal growth rate and glass transition temperature of silicate glasses. *J. Non-Cryst. Solids* **2005**, *351*, 789–794.
- (98) Brock, C. P. High-Z' structures of organic molecules: their diversity and organizing principles. *Acta Crystallogr.* **2016**, *B72*, 807–821.
- (99) Sarma, B.; Roy, S.; Nangia, A. Polymorphs of 1,1-bis(4-hydroxyphenyl)cyclohexane and multiple *Z'* crystal structures by melt and sublimation crystallization. *Chem. Commun.* **2006**, 4918–4920.

- (100) Cruz-Cabeza, A. J.; Reutzel-Edens, S. M.; Bernstein, J. Facts and fictions about polymorphism. *Chem. Soc. Rev.* **2015**, *44*, 8619–8635
- (101) Cote, A.; Erdemir, D.; Girard, K. P.; Green, D. A.; Lovette, M. A.; Sirota, E.; Nere, N. K. Perspectives on the current state, challenges, and opportunities in pharmaceutical crystallization process development. *Cryst. Growth Des.* **2020**, *20*, 7568–7581.
- (102) Kennedy, S. R.; Jones, C. D.; Yufit, D. S.; Nicholson, C. E.; Cooper, S. J.; Steed, J. W. Tailored supramolecular gel and microemulsion crystallization strategies is isoniazid really monomorphic? *CrystEngComm* **2018**, *20*, 1390–1398.
- (103) Taylor, C. R.; Mulvee, M. T.; Perenyi, D. S.; Probert, M. R.; Day, G. M.; Steed, J. W. Minimizing polymorphic risk through cooperative computational and experimental exploration. *J. Am. Chem. Soc.* **2020**, *142*, 16668–16680.